

SANDIA REPORT

SAND2006-6697

Unlimited Release

Printed October 2006

Studies of the Laser-Induced Fluorescence of Explosives and Explosive Compositions

Carol C. Phifer, Randal L. Schmitt, Lawrence R. Thorne, Philip Hargis, Jr.,
and John E. Parmeter

Prepared by Sandia National Laboratories
Albuquerque, New Mexico 87185 and Livermore, California 94550

Sandia is a multiprogram laboratory operated by Sandia Corporation,
a Lockheed Martin Company, for the United States Department of Energy's
National Nuclear Security Administration under Contract DE-AC04-94AL85000.



Issued by Sandia National Laboratories, operated for the United States Department of Energy by Sandia Corporation.

NOTICE: This report was prepared as an account of work sponsored by an agency of the United States Government. Neither the United States Government, nor any agency thereof, nor any of their employees, nor any of their contractors, subcontractors, or their employees, make any warranty, express or implied, or assume any legal liability or responsibility for the accuracy, completeness, or usefulness of any information, apparatus, product, or process disclosed, or represent that its use would not infringe privately owned rights. Reference herein to any specific commercial product, process, or service by trade name, trademark, manufacturer, or otherwise, does not necessarily constitute or imply its endorsement, recommendation, or favoring by the United States Government, any agency thereof, or any of their contractors or subcontractors. The views and opinions expressed herein do not necessarily state or reflect those of the United States Government, any agency thereof, or any of their contractors.

Printed in the United States of America. This report has been reproduced directly from the best available copy.

Available to DOE and DOE contractors from
U.S. Department of Energy
Office of Scientific and Technical Information
P.O. Box 62
Oak Ridge, TN 37831

Telephone: (865) 576-8401
Facsimile: (865) 576-5728
E-Mail: reports@adonis.osti.gov
Online ordering: <http://www.osti.gov/bridge>

Available to the public from
U.S. Department of Commerce
National Technical Information Service
5285 Port Royal Rd.
Springfield, VA 22161

Telephone: (800) 553-6847
Facsimile: (703) 605-6900
E-Mail: orders@ntis.fedworld.gov
Online order: <http://www.ntis.gov/help/ordermethods.asp?loc=7-4-0#online>



SAND2006-6697
Unlimited Release
Printed October 2006

Studies of the Laser-Induced Fluorescence of Explosives and Explosive Compositions

Carol C. Phifer, Randy Schmitt, and Philip Hargis, Jr.
Lasers, Optics, and Remote Sensing Department

Lawrence R. Thorne
Exploratory Systems Technology Department

John E. Parmeter
Contraband Detection Department

Sandia National Laboratories
Albuquerque, New Mexico 87185-0782
Livermore, CA 94550

Abstract

Continuing use of explosives by terrorists throughout the world has led to great interest in explosives detection technology, especially in technologies that have potential for standoff detection. This LDRD was undertaken in order to investigate the possible detection of explosive particulates at safe standoff distances in an attempt to identify vehicles that might contain large vehicle bombs (LVBs). The explosives investigated have included the common homogeneous or molecular explosives, 2,4,6-trinitrotoluene (TNT), pentaerythritol tetranitrate (PETN), cyclonite or hexogen (RDX), octogen (HMX), and the heterogeneous explosive, ammonium nitrate/fuel oil (ANFO), and its components. We have investigated standard excited/dispersed fluorescence, laser-excited prompt and delayed dispersed fluorescence using excitation wavelengths of 266 and 355 nm, the effects of polarization of the laser excitation light, and fluorescence imaging microscopy using 365- and 470-nm excitation. The four nitro-based, homogeneous explosives (TNT, PETN, RDX, and HMX) exhibit virtually no native fluorescence, but do exhibit quenching effects of varying magnitude when adsorbed on fluorescing surfaces. Ammonium nitrate and fuel oil mixtures fluoresce primarily due to the fuel oil, and, in some cases, due to the presence of hydrophobic coatings on ammonium nitrate prill or impurities in the ammonium nitrate itself. Pure ammonium nitrate shows no detectable fluorescence. These results are of scientific interest, but they provide little hope for the use of UV-excited fluorescence as a technique to perform safe standoff detection of adsorbed explosive particulates under real-world conditions with a useful degree of reliability.

Acknowledgments

For assistance in obtaining the explosive materials used in the New Mexico studies, we are indebted to David Hannum, Phil Rodacy, and Mary-Anne Mitchell.

We thank Andrew McCourt for his technical contributions to the laser-induced fluorescence setup. For the technical work done at Sandia/California, we thank Mike Gutzler for his skillful use of the absorption and fluorescence spectrometers and the assembly and use of the fluorescence microscope in acquiring spectra and images of explosives for this study. We also thank George Buffleben for preparing the solid explosives samples for study.

Contents

1	Introduction	11
1.1	Overview	11
1.2	Background	11
2	Description of the Experimental Apparatus	13
2.1	Study of Polarization Effects.....	16
2.2	LIF Imaging Experiments	17
3	Nitro-Based Explosives	18
3.1	Predicted and Previously Reported Photoluminescence Properties of Nitro Explosives.....	18
3.1.1	Intramolecular Electronic Processes	18
3.1.2	Solid-State Effects	20
3.1.3	Fluorescence Quenching by Nitro Explosives	21
3.2	New Photoluminescence Results for Nitro Explosives	22
3.2.1	Spectra Obtained on Bare Gold Substrates	22
3.2.2	Spectra Obtained on Protected Gold Substrates.....	29
3.2.3	Spectra Obtained on Other Substrates.....	31
3.3	Conclusions Concerning Nitro-Based Explosives	33
4	Ammonium Nitrate/Fuel Oil (ANFO)	34
4.1	Properties of Individual Components.....	34
4.1.1	Ammonium Nitrate.....	34
4.1.2	Diesel Fuel.....	36
4.2	Photoluminescence of ANFO.....	39
4.2.1	Effect of Particle Size on Prompt Spectra	41
4.2.2	Delayed Spectra.....	42
4.3	Conclusions Regarding Ammonium Nitrate/Fuel Oil.....	43
5	Polarization Effects	44
5.1	Conclusions from Polarization Studies	47
6	Spectroscopic and Micrographic Fluorescence Surveys	48
6.1	Explosives Studied and Sample Preparation	48
6.2	Absorption Spectra of Explosives	49
6.3	UV-Excited, Dispersed Fluorescence Spectra of Explosives.....	49
6.3.1	Homogeneous Explosives	50
6.3.2	Fluorescence Spectra of AccuStandard Explosives Solutions	51
6.3.3	Fluorescence Spectra of Solid (Dry) Homogeneous Explosives Samples	51
6.3.4	Fluorescence Spectra of Heterogeneous Explosives (ANFO)	54
6.4	Fluorescence Microscopy	57
6.5	Conclusions Concerning Fluorescence of Explosives.....	59
7	Overall Conclusions	59

Figures

Figure 1. Experimental setup for the laser induced fluorescence (LIF) experiments.....	14
Figure 2. Transmission of Barr 420-nm longpass filter used to block the elastically scattered 355-nm laser light while passing the fluorescent light.	15
Figure 3. Timing diagram for prompt laser induced fluorescence (a) and delayed LIF (b)	16
Figure 4. Modified LIF setup used to study the possible effect of polarization	16
Figure 5. LIF imaging setup.....	17
Figure 6. Left, the Jablonski diagram (Lakowicz 1999) for the energy-level ordering of nitrobenzene; center, Jablonski diagram for a nitroarene with a slightly larger aromatic system, and right, nitroarenes with extensive aromatic systems, showing abilities to fluoresce as well as phosphoresce.....	19
Figure 7. Comparison of energy in solution vs. crystal form	20
Figure 8. Prompt LIF spectra of military-grade TNT applied to a gold-coated slide.....	23
Figure 9. Prompt LIF spectra of purified TNT	23
Figure 10. Normalized spectra of purified TNT	24
Figure 11. Comparison of photoluminescence spectrum of Sample 3 of the recrystallized TNT with toluene.....	25
Figure 12. Prompt LIF spectra of TNT Fingerprint on Bare Gold substrate.....	26
Figure 13. Typical prompt LIF spectra observed from the recrystallized TNT samples.....	26
Figure 14. RDX and HMX Prompt Spectra.....	27
Figure 15. Prompt Spectra of RDX and HMX on Bare Gold (normalized)	28
Figure 16. PETN Prompt Spectra	28
Figure 17. PETN Prompt Spectra on Bare Gold.....	29
Figure 18. Intensity drop caused by application of nitro explosives to gold surface.....	30
Figure 19. Prompt Spectra on Protected Gold	30
Figure 20. Protected Gold Substrate	31
Figure 21. Effects of TNT on the fluorescence of painted metal.....	31
Figure 22. Quenching of the fluorescence of white-painted metal.....	32
Figure 23. Quenching of the fluorescence of orange-painted metal.....	32
Figure 24. Prompt LIF spectra from pure NH_4NO_3 , coated NH_4NO_3 , low density ammonium nitrate, and Petro AG	35
Figure 25. Delayed LIF spectra from pure NH_4NO_3 . coated NH_4NO_3 , low-density ammonium nitrate, and Petro AG	36
Figure 26. Prompt LIF spectra of diesel fuel, AccuStandard diesel, and Petro AG.....	37
Figure 27. Delayed LIF spectra of diesel fuel, AccuStandard diesel, and Petro AG.....	37
Figure 28. Prompt and delayed LIF spectra of AccuStandard diesel.	38
Figure 29. Prompt LIF spectra of AccuStandard diesel comparing 266-nm and 355-nm excitation.....	38
Figure 30. Prompt LIF spectra of diesel fuel, ANFO1 sample, and low density ammonium nitrate (266-nm excitation).	39
Figure 31. Prompt LIF spectra of AccuStandard diesel, ANFO2 sample, and low density ammonium nitrate (266-nm excitation).	40
Figure 32. Delayed LIF spectra of diesel fuel, ANFO1 sample, crushed LDAN (266-nm excitation)	40

Figure 33. Delayed LIF spectra of ANFO2 sample, Accustandard diesel, and whole LDAN prills (266-nm excitation)	41
Figure 34. Prompt LIF spectra of AccuStandard diesel, ANFO2 (whole and crushed) and LDAN (266-nm excitation).....	41
Figure 35. Prompt LIF spectra of Accustandard diesel, LDAN (crushed), NaCl (crushed), and Kaolin (powder) (266-nm excitation).	42
Figure 36. Delayed LIF spectra of AccuStandard diesel and ANFO2 (whole and crushed) (266-nm excitation).....	43
Figure 37. Polarized luminescence spectra for pyrolytic graphite.....	44
Figure 38. Four possible configurations for protected gold.....	45
Figure 39. Polarized spectra for a facial tissue	45
Figure 40. Polarized photoluminescence spectra of a PETN fingerprint on protected gold.....	46
Figure 41. TNT powder in Position 1	46
Figure 42. TNT Powder at Position 2, left and Position 3, right	47
Figure 43. Typical absorption spectra for explosives	49
Figure 44. Schematic of how to minimize intensity of light source	50
Figure 45. Fluorescence spectra of the AccuStandard explosives solutions	51
Figure 46. Addition of TNT to the glass cover slips reduced their fluorescence	52
Figure 47. Example of using fused silica cover slips to eliminate background fluorescence	52
Figure 48. Cleaned cover slips show no natural fluorescence	53
Figure 49. Fluorescence of RDX with 210-nm excitation	53
Figure 50. Fluorescence of HMX with 210 nm excitation	54
Figure 51. Fluorescence of PETN with 210 nm excitation.....	54
Figure 52. Fluorescence and absorption of AccuStandard Diesel Fuel.....	55
Figure 53. Fluorescence spectrum of an explosives-grade ammonium nitrate prill soaked with AccuStandard diesel fuel and excited with 210-nm wavelength light.....	55
Figure 54. Photomicrographs of RDX and crushed ammonium nitrate prill particles illuminated with white, 365 and 470-nm light.....	58

Tables

Table 1. Fluorescence of ANFO -ammonium nitrate prill with various exposures to diesel fuel	56
---	----

This page intentionally left blank.

Executive Summary

Standoff detection of large vehicle bombs at safe distances is currently one of the most critical and difficult problems facing the explosives detection community. This LDRD was undertaken to investigate the possibility of using ultra violet (UV), laser-induced fluorescence (LIF) to perform standoff detection of explosives particulates adsorbed on vehicle surfaces. Detection of such particulates could indicate the presence of a vehicle that contains a large mass of explosive material. The explosives studied included the homogeneous explosives, 2,4,6-trinitrotoluene (TNT), 1,3,5-trinitroperhydro-1,3,5-triazine(RDX),1,3,5,7-tetranitroperhydro-1,3,5,7-tetraozone (HMX), pentaerythritol tetranitrate (PETN), and the heterogeneous explosive consisting of ammonium nitrate/fuel oil mixtures (ANFO). The components of ANFO were also studied separately.

Studies of the four nitro-based explosives (TNT, RDX, HMX, and PETN) investigated prompt and delayed fluorescence with excitation primarily at 266 and 355 nm, polarization of both the excitation light and the emitted signals, and fluorescence imaging on a variety of substrates. In all cases, none of these molecules exhibited any significant native fluorescence. Some weak fluorescence signals were observed that could be due to the compounds themselves or to impurities. This result agrees with the limited number of previous studies in the literature, and with theoretical predictions based on the structures of these molecules. This study revealed that all of these nitro-compounds produce a strong quenching effect when adsorbed on various surfaces, for example, protected gold. However, the magnitude of the quenching effect is highly variable, and it is not limited to nitro-based explosives. It is therefore unlikely that this quenching can ever be exploited to produce a robust and accurate method for the standoff detection of adsorbed explosive particulates. Some polarization effects were also observed, but these also were not consistent enough to provide a reliable “fingerprint” for detection.

Ammonium nitrate fluoresces primarily due to the fuel oil, and in some cases, also due to coating materials and/or impurities that are present in the ammonium nitrate. The spectra show some differences depending on whether the ammonium nitrate is in the form of a whole prill or powdered, a particle-size effect that has been observed with other compounds. In general, there does not appear to be a reliable means of distinguishing between ANFO particles and other materials (such fuel oil mixed with dust particles) based on fluorescence spectra.

These results indicate that it is unlikely that laser-induced fluorescence of adsorbed explosive particulates can be used for the standoff detection of large vehicle bombs. While this study is therefore somewhat disappointing from an applications perspective, it still represents, to the best of our knowledge, the most complete survey of the fluorescence properties of these explosives ever performed and is therefore of considerable interest to the wider scientific community.

Acronyms

AN	ammonium nitrate
ANFO	ammonium nitrate and fuel oil mix
C-4	military plastic explosive, 90% RDX, 10% plasticizer
cc	cubic centimeters
cm	centimeter(s)
ft	foot or feet
FWHM	full width at half maximum (used to describe spectrometer resolution)
FO	fuel oil
g	gram(s)
HMX	octogen
ICCD	intensified charge-coupled device
IMS	ion mobility spectrometry
in.	inch or inches
kg	kilogram(s), 1×10^3 g
lb	pound or pounds
LDAN	low density ammonium nitrate
LIF	laser induced fluorescence
LVB	large vehicle bomb
ng	nanogram, 1×10^{-9} grams
NG	nitroglycerine
NM	New Mexico
P_D	probability of detection
PETN	pentaerythritol tetranitrate
RDX	cyclonite
sec	second(s)
Sandia	Sandia National Laboratories
TNT	trinitrotoluene
VBIED	vehicle-borne improvised explosive device

1 Introduction

1.1 Overview

This LDRD was aimed at finding a means of performing standoff detection of explosive particulates adsorbed on vehicle surfaces, a capability that could lead to standoff detection of large vehicle bombs (LVBs). Specifically, the laser-induced fluorescence (LIF) of various key explosives was investigated for this purpose. The work was performed at Sandia National Laboratories/New Mexico and Sandia National Laboratories/California during the course of fiscal years 2005 and 2006, and involved a collaboration among three departments: Lasers, Optics, and Remote Sensing (1128); Exploratory Systems Technology (8134); and Contraband Detection (6418). This report describes the experimental work performed and the results obtained, and discusses the results in relation to previous work in this area.

1.2 Background

Use of explosives by terrorists appears to be a ubiquitous feature of the modern world. For this reason, the development of effective explosives detection technologies is a high priority for the US and many other governments. While close-range detection, for example at checkpoints, represents one very important application, there is a growing need for the ability to detect explosives at substantial distances – so-called standoff detection. Standoff detection would be useful for detecting many types of bombs, but the large vehicle bomb (LVB) represents perhaps the most important threat. Due to the large mass of an explosive that can be contained in a vehicle, the destructive power of an LVB far exceeds that of smaller bombs concealed on people or contained in items such as backpacks. Standoff detection of large vehicle bombs is thus a problem that warrants substantial research and development investment.

As critical as the problem is, the current outlook for standoff detection of explosives is not particularly promising [National Research Council of the National Academies 2004]. Detection of any explosives using any technology is currently difficult at 10 meters, and detection at 100 meters is beyond current capabilities. The discussion below summarizes some techniques that have been used, or might be used, for standoff detection of explosive material, along with some specific pros and cons of the different techniques:

- (1) Backscatter X-ray imaging has been used to image the contents of vehicle cargo holds at distances up to at least 40-60 feet [J. Callerame, American Science and Engineering, private communication; www.as-e.com]. This is certainly a useful capability, but it only provides an image that must be interpreted by an operator and does not specifically identify explosives. Low atomic number (low-Z) materials are distinguishable from high-Z materials such as metals, but not from one another. Furthermore, because the intensities of both the probing X-rays and the backscattered X-rays fall off as $1/r^2$, the total signal intensity of this technique is expected to fall off as $1/r^4$. This will become severely limiting as the standoff distance is increased. Use of this technique in some areas may be limited by concerns over exposing people to even very low doses of X-rays.
- (2) Terahertz/millimeter wave imaging (1 THz = 0.3 mm wavelength) is currently being developed for imaging of bombs concealed on people. This technique is perhaps better

suited than X-ray imaging for personnel screening because the radiation involved is non-ionizing, and the technique can even be passive, i.e. one can simply monitor the radiation emitted from the human body to look for anomalies, rather than actively irradiating a test subject. However, the non-ionizing nature of the radiation makes this technology problematic for vehicle screening, because radiation in this wavelength range will not penetrate metal and thus it is impossible to image what is inside a vehicle cargo hold. Furthermore, like X-ray imaging, this technique will only produce an image that contains possible anomalies – it will not specifically identify explosive materials. Standoff imaging of personnel has recently been demonstrated at distances up to 25 feet [D. McMakin, Pacific Northwest National Laboratory, private communication], and several companies are developing this technology [www.brijot.com, www.sagosystems.com, www.agilent.com, www.qinetiq.com, www.smithsdetection.com, www.l-3com.com].

- (3) Probing neutron technologies such as thermal neutron activation (TNA) and pulsed fast neutron analysis (PFNA) can be used to inspect the contents of vehicle cargo holds. Neutrons are used to irradiate a vehicle being screened, and gamma rays emitted by nuclei inside the vehicle are detected. In contrast to X-ray imaging, these techniques provide some material specificity, TNA identifying nitrogen-rich materials and PFNA being capable of characterizing the amounts of several light elements in a target material. However, the use of this technology for standoff detection is problematic for several reasons. Most notably, there is the same $1/r^4$ dependence of the signal intensity as there is in X-ray imaging. Concerns about exposing people to ionizing radiation are greater than in backscatter X-ray imaging, where the actual doses can be extremely low. The equipment involved is complex and expensive, probably limiting field applications. For all of these reasons, it is unlikely that this technology can be used for standoff detection of large vehicle bombs except possibly in certain specialized circumstances.
- (4) Trained canines have been widely used for explosives detection, and can be very effective in screening vehicles. In principle, dogs can be trained to detect any type of explosive, and they are excellent at following a scent to its source. The biggest drawback of canines is that they cannot operate on a 24/7 basis like a piece of equipment: they generally can work for only a few hours at a time. Furthermore, since they are more like humans than machines, their day to day performance may fluctuate in ways that are not well understood. Dogs can certainly detect explosives at some standoff distance if the mass of explosive is large enough and if not precluded by wind conditions. However, they are generally trained for close-up screening, and thus their ability to detect at various standoff distances is not well characterized.
- (5) Use of trace chemical sensors for standoff detection of large vehicle bombs is problematic for a number of reasons. Most notably, many key explosives have extremely low vapor pressures and the amount of trace material available for sampling is likely to be inadequate to make detections in many cases. This is especially true because the bomb may be packaged and in an enclosed space, limiting the vapor pressure in the plume external to a vehicle to values far below the equilibrium vapor pressure. Recent work at Sandia [Phelan et al. 2005, Lee et al. 2006] has investigated the detection of trace chemical plumes from moving vehicles using chemical preconcentrators and ion mobility spectrometry. In the case of moving vehicles, the plume has a clear directionality, so sampling in the wake of a moving vehicle might hold some promise. Detection of TNT has been demonstrated under some circumstances (TNT in open-bed pickup, tarp-covered

open-bed pickup, or closed sedan trunk) at distances up to at least 45 feet. However, this technique is unlikely to work for low vapor pressure explosives such as RDX, PETN, and HMX, and it is susceptible to cross winds.

The above discussion is not intended to belittle any of these detection techniques. All of these methods are useful for explosives detection under the proper circumstances, and all of them may have something to contribute towards standoff detection. The discussion is intended to point out the difficulty of standoff detection, and the fact that there does not appear to be any “silver bullet” at present that can offer a comprehensive, low-risk solution.

Another potential approach to standoff detection of large vehicle bombs that has been little investigated is the use of probing optical techniques to look for particle contamination on the exterior surfaces of vehicles. Vehicles that have been loaded with large quantities of explosives will contain trace particle contamination on their surfaces in many cases [D. Hannum, unpublished results; C. Ho et al. 2004]. If a laser could be used as the probe, the outgoing signal would not fall off substantially with distance, so the total signal intensity should fall off as the signal from the interrogated particles falls off, probably as $1/r^2$. This is much less distance-limited than a dependence of $1/r^4$. An obvious signal to look for would be fluorescence from the adsorbed particles resulting from laser-induced fluorescence (LIF). It was therefore decided to undertake this LDRD research to investigate LIF as a possible standoff detection technique for large vehicle bombs. It should be noted that other techniques (notably laser-induced breakdown spectroscopy (LIBS) and Raman spectroscopy) are also being investigated currently as a means of performing standoff detection of explosive particulates adsorbed on vehicle surfaces.

2 Description of the Experimental Apparatus

The setup used to perform most of the laser induced fluorescence (LIF) experiments for this LDRD project is shown in Figure 1.

The excitation source is a passively Q-switched Nd:YAG microlaser that produces 2-ns-wide pulses at 120 Hz repetition rate. (The design of this microlaser and its UV conversion system are described in detail Schroder 1999.) The 1064-nm output of the microlaser is frequency converted (using KTP and BBO crystals) to produce 355-nm and 266-nm pulses with several μJ /pulse energy at each wavelength. A Pellin-Broca prism is used to disperse the coaxially transmitted wavelengths and an iris is used to select which excitation wavelength illuminates the sample. Neutral density filters (not shown) are used to attenuate the pulse energy as needed to avoid saturation effects.

Laser induced fluorescence (as well as other light scattered) from the sample is collected by a set of UV achromats and imaged with 1:1 magnification onto the entrance slit of an imaging spectrograph (Jobin-Yvon CP-140). The concave diffraction grating of the CP-140 disperses the collected light and forms a 25-mm-long flat-field spectrum in its back focal plane. This spectrum is recorded by an intensified CCD (Princeton Instruments IMAX ICCD system) camera. The ICCD allows time-gated acquisition of the collected spectrum both to reduce background light and to allow some degree of discrimination between prompt and longer-lived fluorescence.

This spectrograph/ICCD system is configured to record spectral data from ~315 nm to ~750 nm and with a 0.5-mm-wide slit has a measured spectral resolution of ~10 nm (FWHM).

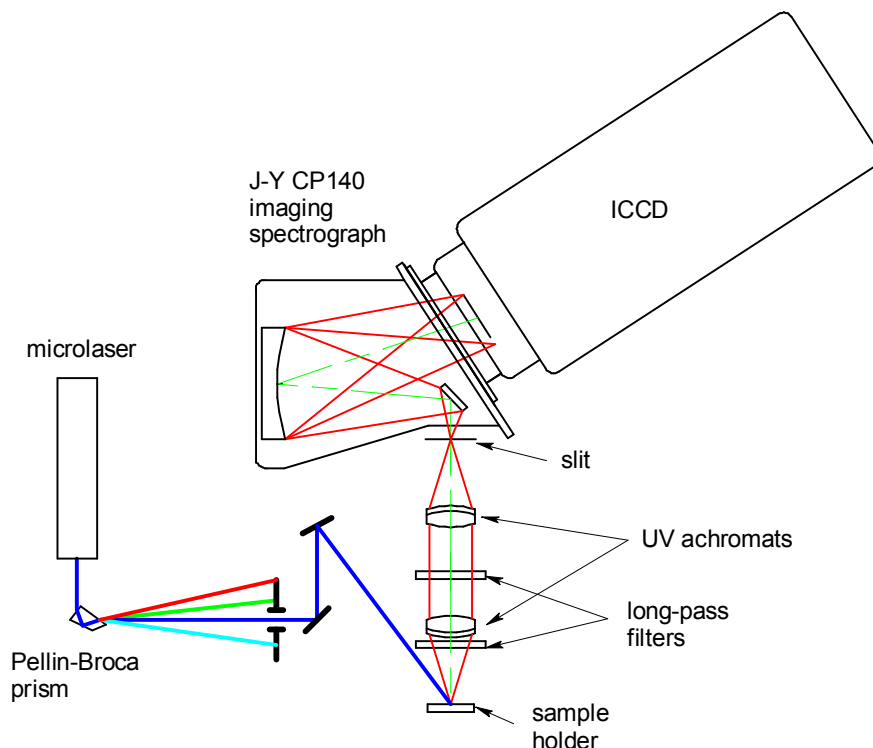


Figure 1. Experimental setup for the laser induced fluorescence (LIF) experiments

The main drawback to using a microlaser for LIF measurements is that the pulse-to-pulse timing jitter inherent in passively Q-switched lasers (± 50 ns in this case) limits the ability to use time delay gating to observe prompt (within a few ns of excitation) fluorescence without interference from the (huge) elastically scattered signal from the excitation laser. In principal, one can trigger the ICCD gating electronics from the laser pulse itself and have virtually no effect from pulse timing jitter. Unfortunately, the signal propagation delay through the pulse timing generator and the ICCD gating circuit limits the shortest delay from the laser pulse firing to the ICCD gate opening to 100 ns. In many cases, the fluorescence lifetime for species of interest are of the order of several to 10 ns. In order to observe truly prompt fluorescence, the team gated the ICCD detector “on” before the laser pulse (as described below) and used a long-pass filter to block the elastically scattered light.

For this work, we used a set of custom multilayer dielectric long-pass filters (designed and fabricated by Barr Associates) to block elastically scattered laser light from entering the spectrograph and pass the longer-wavelength fluorescence. These filters work by efficiently reflecting the wavelengths to be blocked, not by absorbing any light. Figure 2 shows the transmission vs. wavelength for the Barr 420-nm long-pass filter which was used to block the 355-nm laser light when it was used as the LIF excitation source. In this case, the filter turn-on wavelength, defined as the 50% transmission point, is 420 nm. A similar filter which turns on at

320 nm was used to block the 266-nm laser light when it was used as the LIF excitation source. It is important to point out that absorptive long-pass (and other colored-glass) filters are unacceptable for use in high-sensitivity laser induced fluorescence work because the filters themselves can fluoresce as a result of absorbing laser light. This instrument-related background fluorescence from colored-glass filters can overwhelm (or at least seriously contaminate) the relatively weak LIF from samples under study. One must also be very careful with any of the instrument surfaces that may receive direct or scattered laser light as these are all a potential source of unwanted instrument-related fluorescence signals.

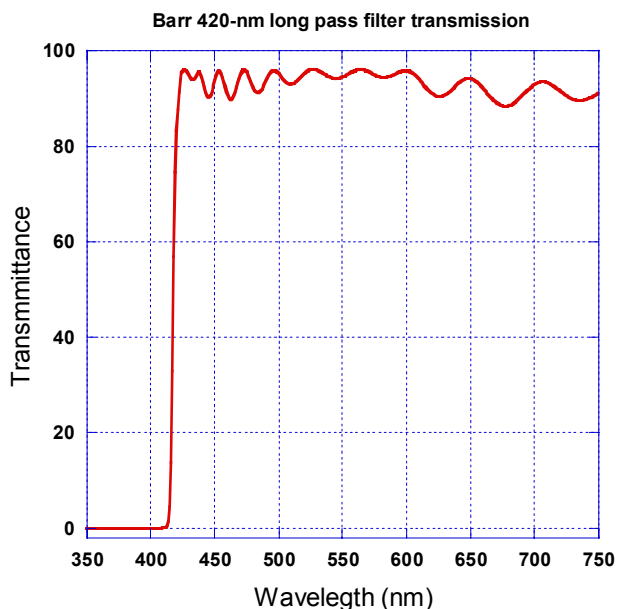


Figure 2. Transmission of Barr 420-nm longpass filter used to block the elastically scattered 355-nm laser light while passing the fluorescent light.

Pulsed laser excitation combined with time-gated detection (ICCD) allows this system to record both the prompt and delayed fluorescent emission from the samples and also allows the fluorescence lifetime to be measured. Figure 3 shows the timing diagram used to record both prompt (a) and delayed (b) fluorescence. To record prompt fluorescence, we relied on two long-pass filters (described above) to block the elastically scattered light (since the laser timing jitter prevents direct temporal gating to eliminate the elastically scattered light). As illustrated in Figure 3 (a), the ICCD was typically gated “on” with a 2- μ s-wide gate approximately centered at the time of the (\sim 2-ns-wide) laser pulse. This timing ensured that even with \pm 50 ns jitter (and the larger, slow drift of the average pulse build-up time), the laser pulse would always be inside the ICCD gate, and, as a result, the prompt fluorescence could be recorded.

The timing diagram for recording delayed fluorescence is shown in Figure 3 (b). Here the laser pulse itself is used to trigger the timing and gating electronics resulting in a minimum delay between the laser pulse and the opening of the ICCD gate of 100 ns. Typically, for delayed fluorescence measurements, we used a 100- μ s-wide gate with a 100-ns delay from the excitation pulse as shown in the figure.

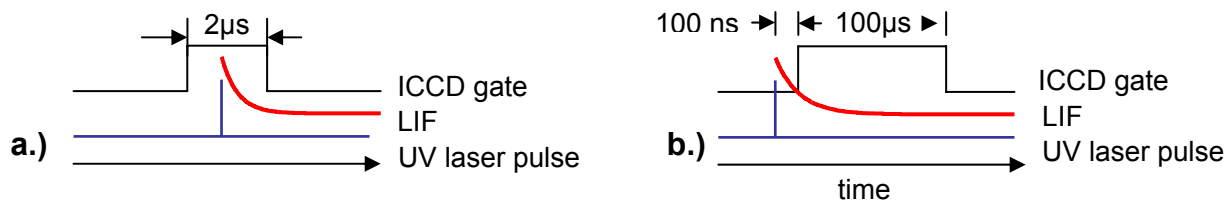


Figure 3. Timing diagram for prompt laser induced fluorescence (a) and delayed LIF (b)

2.1 Study of Polarization Effects

Fluorescence is generally an isotropic process, emitting photons in all directions with random polarization. However, in some cases, the structure of the molecules and/or their interactions with the surfaces they are in contact with can produce an anisotropy with respect to polarization in the absorption or emission process (i.e., either preferentially absorbing one polarization state or preferentially emitting in one polarization). To explore the possibility of using polarization as a way to enhance the detection or at least increase the contrast with respect to an isotropic fluorescent background, we modified the LIF apparatus to allow control of the input polarization and analysis of the emission polarization. The modified LIF setup is shown in Figure 4.

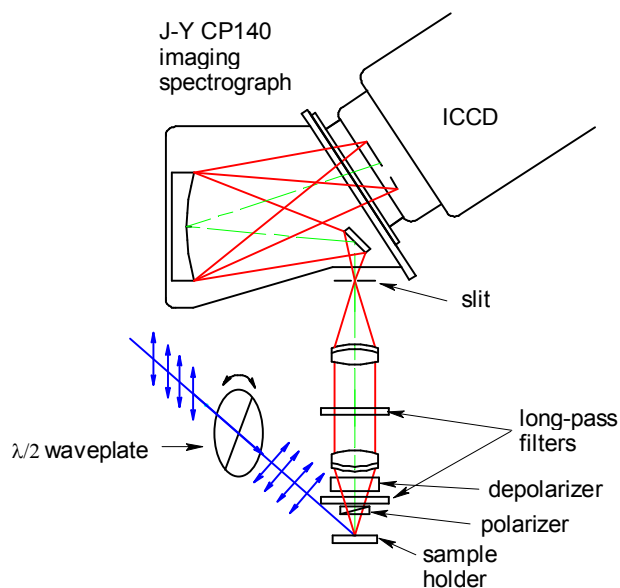


Figure 4. Modified LIF setup used to study the possible effect of polarization

Since the 355- and 266-nm laser light is already linearly polarized, we added a $\lambda/2$ waveplate to allow arbitrary rotation of the polarization of the light incident on the sample. (There is actually a separate waveplate for 266 nm and 355 nm, and the appropriate waveplate is installed in the setup depending on the excitation wavelength.) For linearly polarized input light, the $\lambda/2$ waveplate only rotates the direction of polarization, preserving its linear polarization state. In general, we oriented the $\lambda/2$ waveplate to make the input polarization either parallel to the plane of incidence (p-polarized light) or perpendicular to the plane of incidence (s-polarized light). The

plane of incidence is defined by the plane containing the incident and reflected laser beams. To analyze the state of polarization of the fluorescent emission from the samples, we used a high-quality dichroic polarizer that could be rotated. We aligned the transmission axis of the analyzer polarizer to be either parallel or perpendicular to the excitation polarization direction. Because the efficiency of a diffraction grating depends on polarization, we used a depolarizer to scramble the polarization of the input to the spectrometer. This eliminates any instrument-related polarization sensitivity. All other components of the LIF system (such as the long-pass filters and sample holder) were kept the same.

2.2 LIF Imaging Experiments

Another potential approach to LIF detection of explosives on surfaces is to image an area and look for contrast between fluorescent and non-fluorescent regions. Since nitro-based explosives are such good quenchers of fluorescence, and since many common surfaces (especially vehicles) are fluorescent, the study investigated whether or not fluorescent imaging could identify the presence of explosives on surfaces. The team built a fluorescence imaging system, shown in Figure 5, consisting of an Andor ICCD (similar in performance and design as the Princeton Instruments ICCD used for the spectrally dispersed LIF measurements) coupled to a CCTV lens.

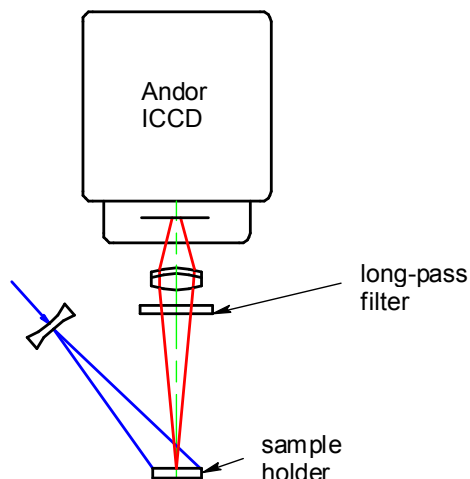


Figure 5. LIF imaging setup

The team used the same long-pass filters as in the spectrally dispersed instrument to reject the elastically scattered laser light and pass the fluorescent emission from the sample. The micro-laser excitation beam was expanded using a lens system and the sample was broadly illuminated (over ~50-mm-diameter area). The CCTV lens collected light scattered from the sample and imaged it onto the photocathode of the ICCD. The Andor ICCD was gated for prompt and delayed fluorescence measurements as described before (Figure 5).

3 Nitro-Based Explosives

The following section outlines some theoretical considerations and previous work on absorption and photoluminescence from nitro-based explosives and describes the experimental results from this LDRD project for laser induced fluorescence from these compounds. Refer to the appendix for a summary of previously reported absorption/reflectance spectral data.

3.1 Predicted and Previously Reported Photoluminescence Properties of Nitro Explosives

3.1.1 Intramolecular Electronic Processes

The nitro-based explosives under consideration are molecular compounds, and their optical properties in the gas phase or in solution are due to electronic transitions within individual molecules. The following discussion focuses on the energy levels that would be involved in any photoluminescence resulting from intramolecular processes.

3.1.1.1 Nitroarenes

Nitroarenes, or nitroaromatics, are compounds in which one or more nitro groups are attached to aromatic rings. Examples include nitrobenzene, TNT, and 1-nitronaphthalene. The following discussion will distinguish between two types of photoluminescence: 1) fluorescence, which is a transition occurring from the lowest excited singlet state to the ground singlet state, and 2) phosphorescence, which refers to a formally forbidden transition from the lowest excited triplet state to the singlet ground state (Lower and El-Sayed 1966). Most nitroarenes are known to lack fluorescence (Khalil et al. 1970; Ohtani et al. 1980), but some of them can show weak phosphorescence, especially at cryogenic temperatures. Nitroarenes exhibit fluorescence only if the aromatic system is large.

The left side of Figure 6 shows the Jablonski diagram (Lakowicz 1999) for the energy-level ordering of nitrobenzene, a mononitroarene with a small aromatic system. The absence of fluorescence is due primarily to the high efficiency of the intersystem crossing (ISC) from the singlet n,π^* state to the triplet π,π^* state (Lower and El-Sayed 1966). The low-lying n,π^* levels are due to the presence of nonbonding lone-pair orbitals on the oxygen atoms of the nitro group. It has been suggested that the fast ISC of nitroarenes is caused by strong coupling between the excited singlet and triplet states, both of which show large distortions of the nitro group relative to the geometry of the ground state (Takezaki et al. 1998; Takezaki et al. 1997b). Nitrobenzene also shows no phosphorescence, due to the short lifetime of the lowest excited triplet state (Takezaki et al. 1997a). It can be concluded that related small nitroarenes with multiple nitro groups, such as TNT, would not be expected to exhibit either fluorescence or phosphorescence. The center diagram in Figure 6 gives the Jablonski diagram for a nitroarene with a slightly larger aromatic system—for example, 1-nitronaphthalene. As in nitrobenzene, no fluorescence occurs because of the dominance of the nonradiative ISC; however, phosphorescence is observed at 77 K (Khalil et al. 1970). Phosphorescence occurs from the triplet π,π^* state (primarily located on the aromatic system), which in this case is lower in energy than the triplet n,π^* state.

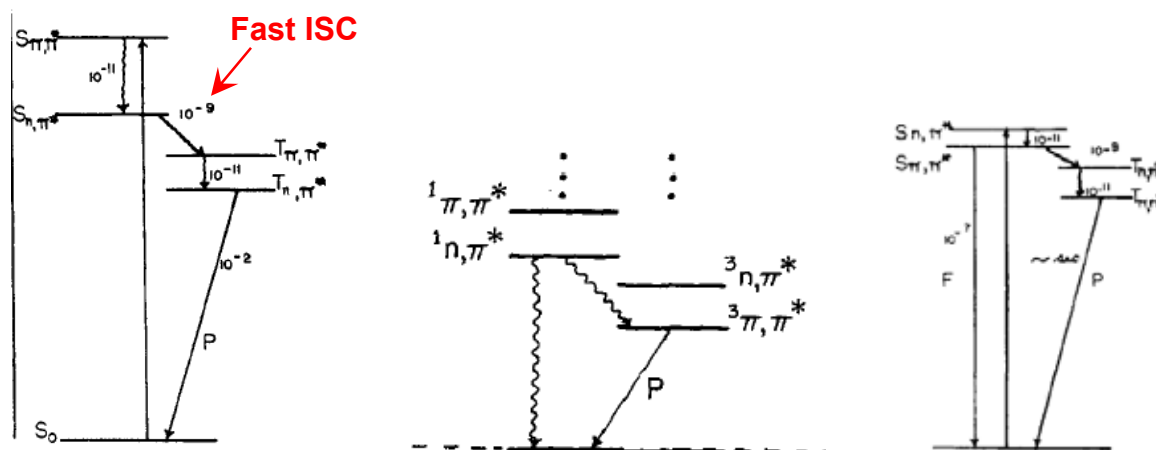


Figure 6. Left, the Jablonski diagram (Lakowicz 1999) for the energy-level ordering of nitrobenzene; center, Jablonski diagram for a nitroarene with a slightly larger aromatic system, and right, nitroarenes with extensive aromatic systems, showing abilities to fluoresce as well as phosphoresce

For nitroarenes with extensive aromatic systems (such as 6-nitrochrysene), the singlet π,π^* state becomes lower in energy than the singlet n,π^* state, which allows fluorescence to occur in addition to phosphorescence (Khalil et al. 1970). This situation is shown at the right of Figure 6.

In summary, explosive nitroarenes such as 1,3,5-trinitrobenzene, 2,4,6-trinitrotoluene, and tetryl are not expected to exhibit detectable luminescence, especially at room temperature. It is possible that explosives with larger aromatic systems, such as 2,2',4,4',6,6'-hexanitrostilbene or some of the photoproducts of TNT, could show some weak luminescence.

3.1.1.2 Aliphatic Nitramines

The cyclic aliphatic nitramine explosives RDX and HMX do not possess the conjugated π systems found in the nitroarenes. The nitro groups have π orbitals, but the σ , n , and π orbitals are so intimately mixed in the nitramine molecules (Stals et al. 1969) that there is no clear delineation among them; this is presumably due to the N-N bonding between the nitrogens in the NO_2 groups and the nitrogen atoms of the ring. The nitramines' lowest excited singlet states are at higher energies than those of the nitroarenes (Smith et al. 1984; Stals et al. 1969). In fact, intense excitation into the nitro-group absorption band of the nitramines causes photodecomposition (Marinkas 1975, Marinkas 1977), which is one explanation for their lack of photoluminescence in solution.

3.1.1.3 Aliphatic Nitrate Esters

As opposed to the nitramines, in which the NO_2 groups are attached to nitrogen atoms, the nitrate esters such as PETN contain NO_2 groups bonded to oxygen atoms. The observable electronic transitions in the aliphatic nitrate esters are essentially localized on the nitro groups. The lowest excited state, whose absorption band occurs at about 290 nm, is of n,π^* character, but the strongest absorption is to the π,π^* state at about 194 nm (Mullen and Orloff 1973). In ethyl nitrate, a compound used to approximate PETN, the lowest triplet level is also the n,π^* state. Therefore, the energy-level diagram for PETN probably looks similar to that shown above for nitrobenzene,

with the π,π^* states residing on the nitro groups rather than on an aromatic ring and consequently located at higher energies relative to the ground state. In analogy with nitrobenzene, fluorescence would not be expected, and phosphorescence would be possible but not probable.

3.1.2 Solid-State Effects

In the solid state, both intermolecular interactions and crystal defects can give rise to electronic states that are modified or in addition to the intramolecular energy levels. The nitro groups appear to be responsible for intermolecular cohesion in the solid state (Kuklja and Kunz 2000), and the intermolecular interactions in nitro explosives are thought to play an important role in their thermal decomposition and detonation behavior (Brill and James 1993, Zeman and Krupka 2003). Intermolecular electrostatic interactions are significant because of alternating relatively negative (oxygen atoms) and positive (carbon and nitro-group nitrogen atoms) charges on nearby molecules in the crystal (Karpowicz and Brill 1983). The major intermolecular attractions in RDX are between O and N, while in HMX they are primarily between O and C (Karpowicz and Brill 1983). Intermolecular hydrogen bonding occurs in solid HMX (Allis et al. 2006), in TNT between the ring hydrogens and neighboring nitro groups (Carper et al. 1982, Nash et al. 1989), and in PETN between the oxygens and the CH_2 hydrogens (Brand 2005). In addition to short-range intermolecular interactions, the presence of longer-range defects such as edge dislocations in the crystals reduces the optical band gap and thereby affects absorption and luminescence properties (Kuklja and Kunz 2001).

Solid-state luminescence effects have been studied for the nitramines. The electronic spectra of the nitramines differ according to whether they are obtained in solution (isolated molecules) or as crystals. In solid form, the nitramines exhibit a weak absorption band in the near-UV ($\sim 355\text{-}365$ nm) which has been assigned to a charge-transfer (CT) state arising from the formation of intermolecular complexes (Marinkas 1975, Marinkas 1977, Marinkas et al. 1976, Stals 1971). These complexes may be associated with the formation of defects at crystal surfaces.

The energy-level diagram of Figure 7 shows that the excited singlet CT state is appreciably lower in energy than the lowest excited singlet state found in the solvated molecules (Marinkas 1977).

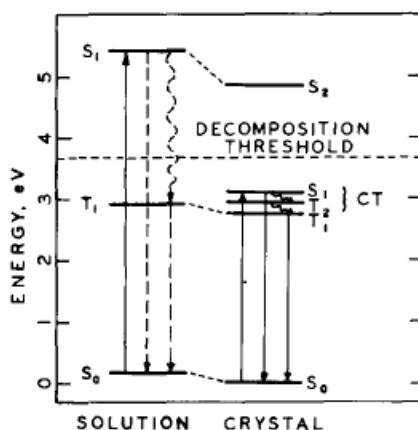


Figure 7. Comparison of energy in solution vs. crystal form

Weak, short-lived fluorescence has been detected from this singlet CT state at room temperature, and the corresponding fluorescence excitation spectrum agrees well with the CT absorption band (Marinkas 1975). Phosphorescence at 77 K has also been observed. The fact that there are two phosphorescence lifetimes indicates the existence of two excited triplet states with similar energies. One may be associated with monomeric emission and the other with CT emission (Marinkas 1977). The photolytic decomposition threshold shown in Figure 7 is at about 340 nm. The details of the nitramine photoluminescence are given below:

HMX – Solution

(Marinkas 1975)

None observed

HMX – Solid

(Marinkas 1975, Marinkas 1977)

At 300 K: $I_{\max} \approx 472$ nm, $\tau < 3.5$ ns

Deuterated $I_{\max} \approx 472$ nm

At 77 K: $I_{\max} \approx 515$ nm, $\tau_1 = 60$ ms, $\tau_2 = 400$ ms, quantum efficiency $\approx 6 \times 10^{-3}$ - 6×10^{-2}

Deuterated $I_{\max} \approx 505$ nm, $\tau_1 = 90$ ms, $\tau_2 = 570$ ms

RDX – Solution

(Marinkas 1975, Stals et al. 1969)

None observed

RDX – Solid

(Marinkas 1975, Marinkas 1977)

At 300K: $I_{\max} \approx 463$ nm, $\tau < 3.5$ ns, quantum efficiency $\approx 10^{-2}$ - 10^{-1}

Deuterated $I_{\max} \approx 474$ nm

At 77 K: $I_{\max} \approx 525$ nm, $\tau_1 = 120$ ms, $\tau_2 = 480$ ms, quantum efficiency $\approx 4 \times 10^{-3}$ - 4×10^{-2}

Deuterated $I_{\max} \approx 520$ nm, $\tau_1 = 160$ ms, $\tau_2 = 720$ ms

It may be that solid PETN can exhibit intermolecular CT states analogous to those of the nitramines. Like the nitramines, powdered PETN shows increased long-wavelength absorption relative to the solution spectra (Smit 1991). It has been reported that the photoluminescence of PETN has a very low quantum yield (Dreger et al. 2002). The wavelength of the maximum emission intensity is about 420 nm (Dreger et al. 2002), which is in the region that would be expected for any CT emission similar to what is seen for the nitramines.

In summary, either weak photoluminescence or none at all is expected at room temperature for typical nitro-based explosives. Any intrinsic luminescence observed for these materials under ambient conditions would most likely be due to solid-state effects.

3.1.3 Fluorescence Quenching by Nitro Explosives

Nitro-containing compounds are known to act as effective fluorescence quenchers in solution (Goodpaster and McGuffin 2001), a process known as dynamic or diffusional quenching which involves the formation of a transient excited-state complex. When a solid nitro compound is adsorbed onto a substrate, any resulting decrease in the fluorescence of the substrate would be due to static quenching, which results from the formation of a ground-state complex between the fluorophore (substrate) and the quencher (nitro compound). Little is known about the static

quenching properties of nitro compounds, but recently it has been shown that the fluorescence of thin films of conjugated polymers is quenched upon exposure to vapor-phase nitroaromatic explosives (Toal and Trogler 2006). It is known in general that static quenching of fluorescence is usually much more effective than dynamic quenching and can result in substantially lower detection limits (Rakicioglu et al. 1998).

The efficiency of the fluorescence quenching of pyrene in solution decreases in the following order: TNT > RDX > PETN > HMX (Goodpaster and McGuffin 2001). This agrees with a previous observation that the fluorescence quenching efficiency of the nitramines (HMX and RDX) is less than that of the nitroaromatics such as TNT (Wallenborg and Bailey 2000).

3.2 New Photoluminescence Results for Nitro Explosives

The laser-induced fluorescence (LIF) spectra shown in this section were obtained using the instrumental setup described in Section 2 and illustrated in Figure 1. As discussed in Section 2, this LIF setup uses a short-pulse (~2 ns) laser and a time-gated ICCD detector both to minimize background light and to allow discrimination between short-lived and long-lived emission. The timing diagram that shows the ICCD gate timing with respect to the laser excitation pulse is shown in Figure 3.

3.2.1 Spectra Obtained on Bare Gold Substrates

In order to minimize the amount of fluorescence from interferences, fused-quartz slides coated with gold were used as substrates. In previous LIF work, fused-quartz slides coated with bare gold were found to have an essentially negligible fluorescence background, allowing the study of any luminescence arising from the nitro explosives themselves. All the spectra in this section are “prompt,” since there is little or no delayed emission observed from the nitro explosives on bare gold substrates, even at a delay time of only 100 ns.

3.2.1.1 TNT Excited at 266 nm

Figure 8 shows spectra taken at 6 different locations on a “fingerprint” of military-grade TNT applied to a slide coated with bare gold. The excitation wavelength was 266 nm. It is evident that there is a great deal of position-dependent spectral variability.

Positions 2, 3, and 5 have the shortest-wavelength maxima, Position 4 has its maximum intensity in the range 415-440 nm, and Positions 1 and 6 show a broad luminescence peaking in the 540-590 nm region. Of course, the full extent of the short-wavelength peak is not obtained because of the presence of the 320-nm longpass filters. In an effort to differentiate between intrinsic TNT signals and those due to impurities, the spectra of several small (~1 mm) pieces of recrystallized (*i.e.*, purified) TNT were obtained. These are shown in Figure 9.

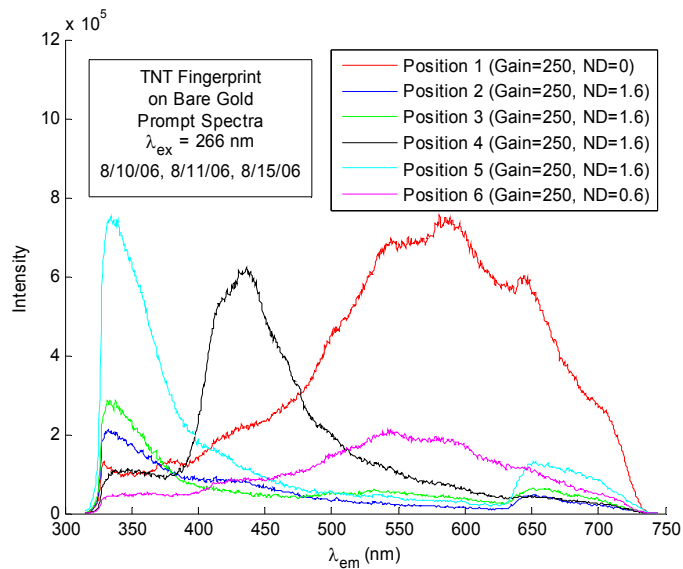


Figure 8. Prompt LIF spectra of military-grade TNT applied to a gold-coated slide

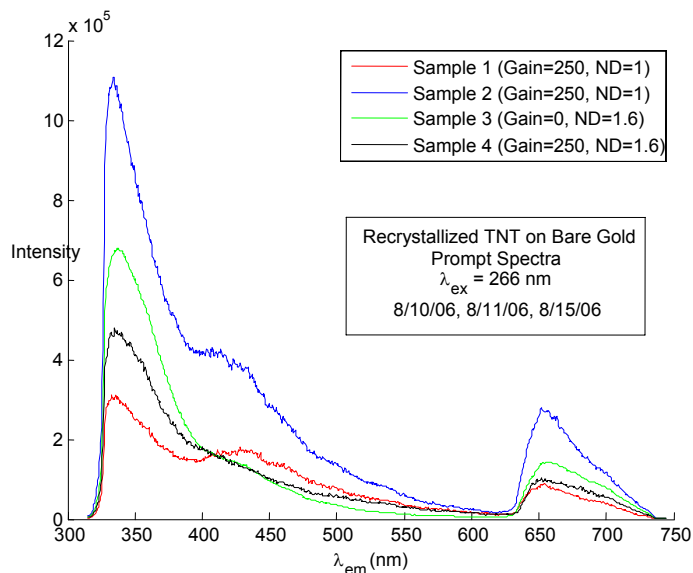


Figure 9. Prompt LIF spectra of purified TNT

Figure 10 shows the normalized version of Figure 9.

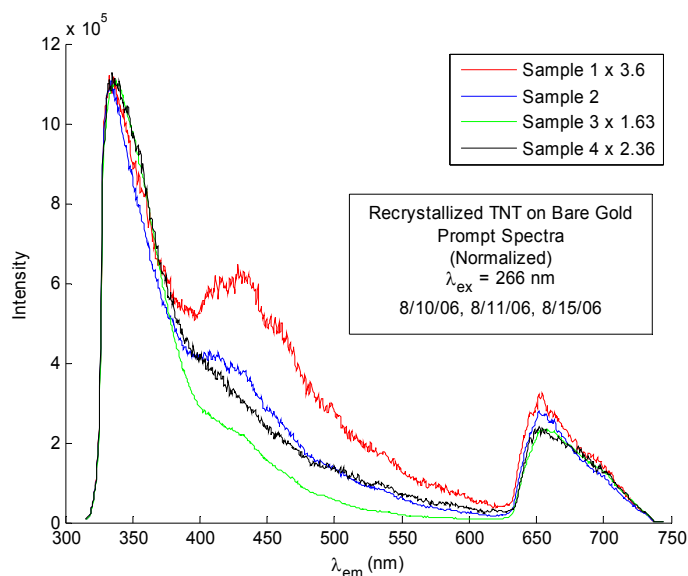


Figure 10. Normalized spectra of purified TNT

These spectra show more uniformity. In all cases, the purer form of TNT shows only the high-frequency band and a smaller band centered at about 425 nm. There is a range of relative intensities of the 425-nm peak, which could indicate that it is 1) easily degraded by the laser, 2) caused by a photoproduct of TNT, 3) due to an impurity, or 4) highly dependent on the surface properties of the sample. (The asymmetric peak at about 650 nm is part of the spectrum observed in the second order of the spectrometer grating.) The fact that the 425-nm band was apparently detected as a stand-alone feature in the TNT fingerprint sample (Position 4 of Fig. 3-5) suggests that it is not intrinsic to TNT but is instead due to an impurity. Similarly, the broad long-wavelength emission detected from Positions 1 and 6 in Fig. 3-5 are not seen in the spectra of the recrystallized TNT and therefore can be assumed to arise from unidentified impurities.

The conclusion is that if TNT does show any intrinsic photoluminescence when excited at 266 nm, its intensity is relatively weak and its λ_{max} is at a wavelength shorter than 320 nm. The fact that nitrobenzene, with only one nitro group, shows no detectable photoluminescence implies that any emission from pure crystalline 2,4,6-trinitrotoluene would be caused either by solid-state effects or by photoproducts.

Laser excitation of nitrobenzene vapor at 260 nm produces considerable fluorescence that has been identified as arising from the formation of benzene as a photochemical byproduct (Ahmad and Foster 2000). If a similar process were to occur during the laser irradiation of TNT at 266 nm, the expected photoproduct would be toluene. Figure 11 compares the photoluminescence spectrum of Sample 3 of the recrystallized TNT with that of toluene dissolved in cyclohexane (Fuh 1995).

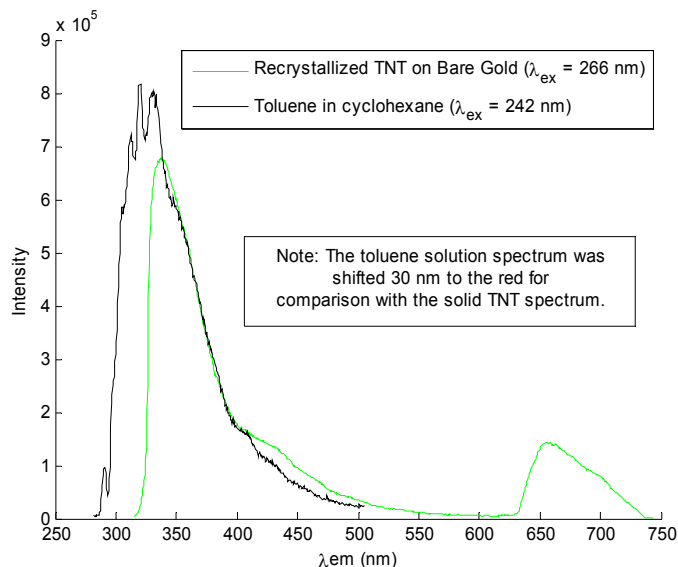


Figure 11. Comparison of photoluminescence spectrum of Sample 3 of the recrystallized TNT with toluene

The toluene spectrum has been moved 30 nm to the red; such a bathochromic shift is typically seen for solid-state spectra relative to solution spectra. If a small amount of toluene were being formed from the TNT during excitation, it probably would be adsorbed to the surface of the solid or trapped in the matrix; both conditions would be expected to cause changes in the emission spectrum relative to the solution state. The similarities of the spectra in Fig. 3-8 give a possible explanation for the photoluminescence observed from recrystallized TNT. It can also be noted here that no delayed (> 100 ns) luminescence was observed for TNT, and the fluorescence lifetime of toluene is only 34 ns (Berlman 1971).

3.2.1.2 TNT Excited at 355 nm

Using an excitation wavelength of 355 nm seems to avoid degradation of the TNT. Two representative spectra from a fingerprint of TNT show two main peaks: one is partially obscured by the longpass filter, and the other occurs at about 550-560 nm. The higher-frequency peak may be due to small amounts of toluene from photodegradation caused while exciting at 266 nm. Positions 1 and 6 in Figure 8 (excitation at 266 nm) have bands that resemble the 550-560 luminescence of Figure 12.

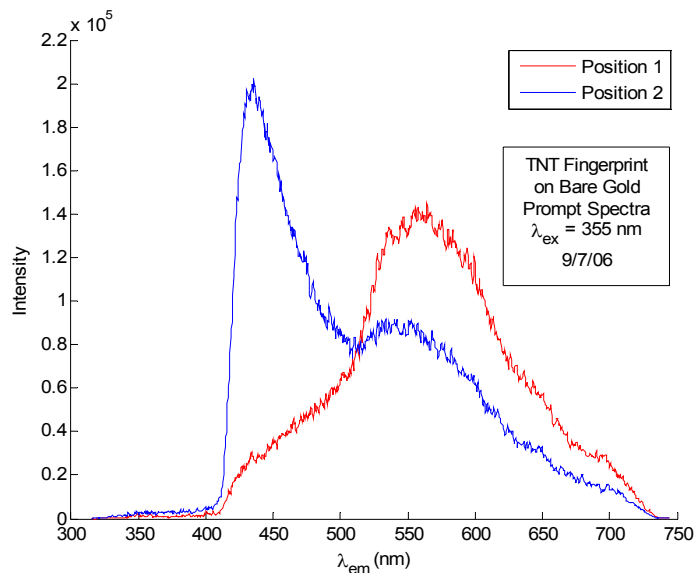


Figure 12. Prompt LIF spectra of TNT Fingerprint on Bare Gold substrate

Typical spectra observed from the recrystallized TNT samples are shown in Figure 13. The spectra are normalized according to their higher-intensity peaks (except for the bare gold spectrum, shown for reference). The two main features observed in the fingerprint sample are also seen here in the purer samples. It is possible that the 560-nm band arises from the TNT itself; however, it is not seen in every sample. As stated previously in this report, any intrinsic photoluminescence from TNT would most likely be due to solid-state intermolecular effects rather than intramolecular processes.

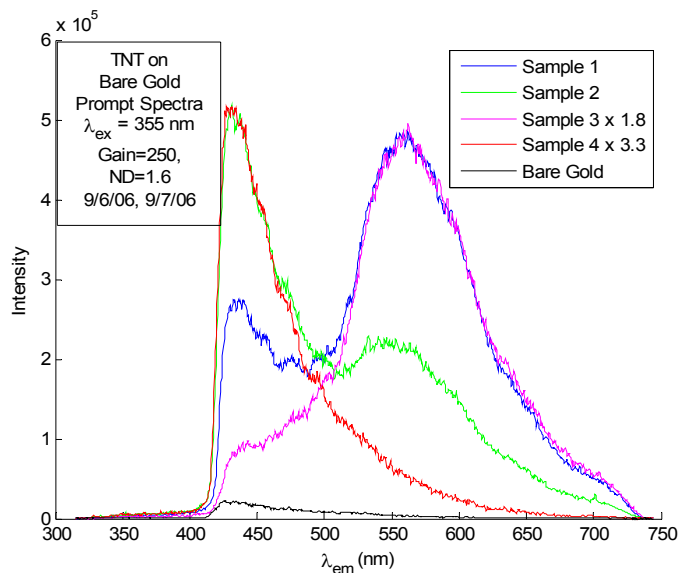


Figure 13. Typical prompt LIF spectra observed from the recrystallized TNT samples

3.2.1.3 Nitramines (RDX and HMX) Excited at 266 nm

As with TNT, a great deal of variability occurs on the fingerprint samples of the nitramines RDX and HMX. These two compounds differ only in ring size and number of nitro groups. RDX has three nitro groups, and the larger ring of HMX is connected to four nitro groups. The room-temperature emission maxima have been reported (Marinkas 1975, Marinkas 1977) as 463 nm for solid RDX and 472 nm for solid HMX, but the photolytic decomposition threshold occurs at 340 nm. Therefore, no photoluminescence would be expected with an excitation wavelength of 266 nm. Position 1 of the RDX sample, which is similar to the HMX spectra, has a λ_{max} of 402 nm, while all three of the HMX spectra have maxima at about 426 nm. (See Figure 14.)

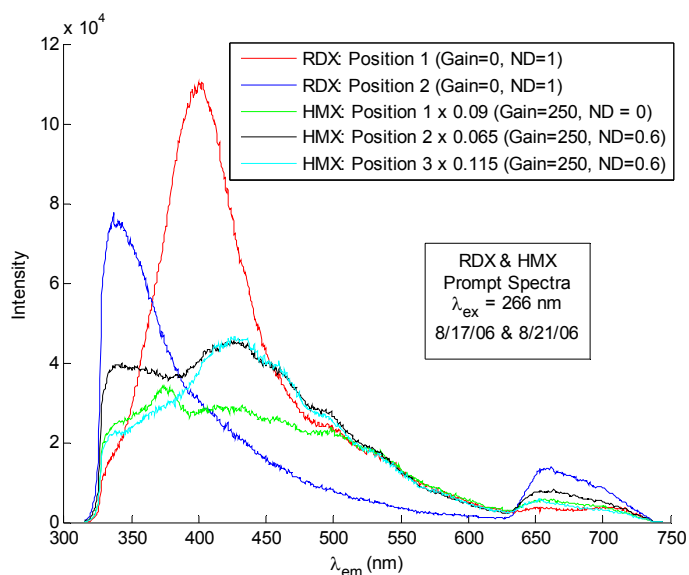


Figure 14. RDX and HMX Prompt Spectra

Apparently, these samples contain impurities introduced during synthesis or processing, or else some luminescence is arising from the photodissociation byproducts.

3.2.1.4 Nitramines (RDX and HMX) Excited at 355 nm

The spectra excited at 355 nm would not be expected to contain contributions from photo-products, since that wavelength is longer than the dissociation threshold. However, neither of the 463-nm and 472-nm luminescence maxima reported by Marinkas is observed (Figure 15).

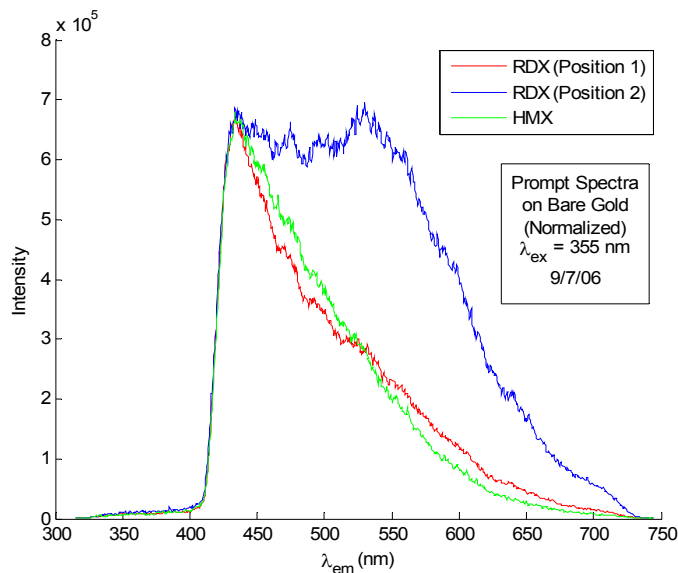


Figure 15. Prompt Spectra of RDX and HMX on Bare Gold (normalized)

3.2.1.5 PETN Excited at 266 nm

In agreement with the reported λ_{max} of about 420 nm for PETN (Dreger et al. 2002), Figure 16 shows intensity maxima at 429 for Position 2 and 419 for Position 3. Apparently the only previously published emission spectrum for PETN appeared in a book of Russian-language conference proceedings (Krysanova et al. 2004), but the book is out of print and could not be obtained.

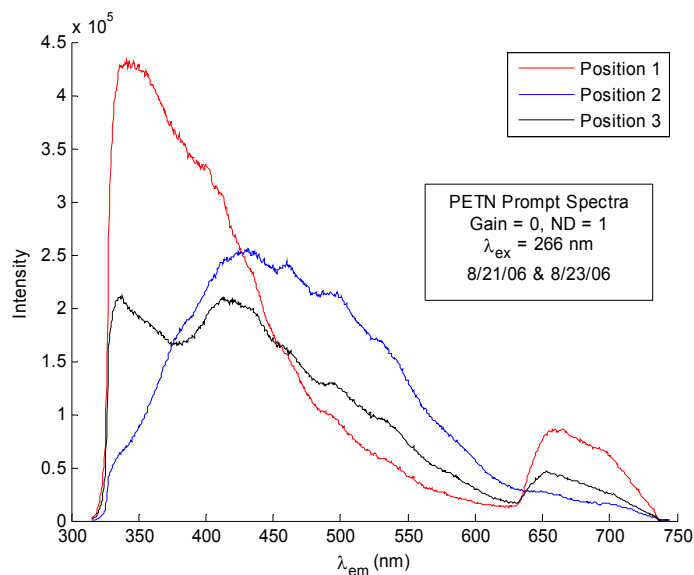


Figure 16. PETN Prompt Spectra

It is not known whether the PETN luminescence is intrinsic. The spectra of PETN Positions 2 and 3 resemble the HMX spectra of Figure 14.

3.2.1.6 PETN Excited at 355 nm

The spectra excited at 355 nm on bare gold (Positions A and B in Figure 17) are fairly featureless and do not show any additional information relative to the 266-nm spectra.

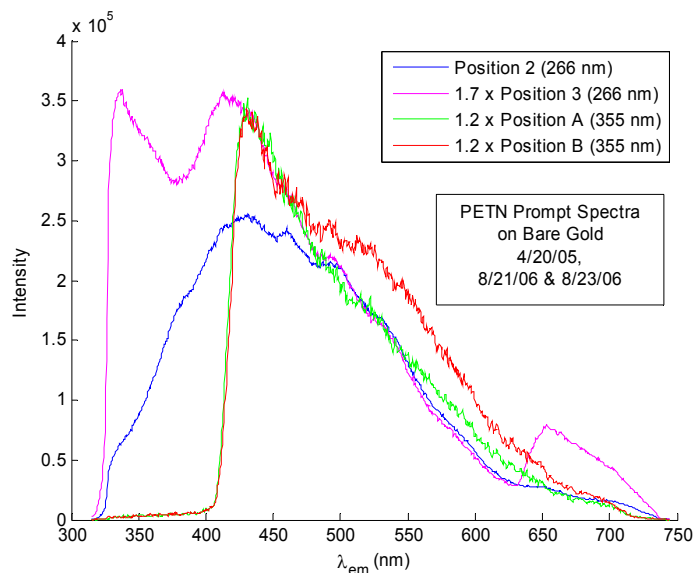


Figure 17. PETN Prompt Spectra on Bare Gold

3.2.2 Spectra Obtained on Protected Gold Substrates

The protected gold (PG) surface is coated with a thin layer of MgF_2 . Whereas the bare gold surface does not make a significant contribution to the photoluminescence spectra, the fluorescence from the protected gold was easily detectable under the experimental conditions used for this report. The main effect of the presence of nitro-based explosives on the PG surface is a quenching of the fluorescence from the protected gold.

3.2.2.1 Prompt Spectra

Figure 18 shows the dramatic drop in intensity caused by the application of nitro explosives to a protected gold surface. All the spectra were prompt, excited at 355 nm, and taken with the same instrumental settings. Perhaps fortuitously, the relative heights of the peaks are in the same order as would be expected from the dynamic quenching efficiencies mentioned in Section 3.2.3.

In general, when the fluorescence of the protected gold is quenched by the nitro explosives, the basic shape of the PG spectrum is preserved; its intensity is simply reduced. This can be seen in Figure 19, the normalized version of Figure 18. TNT is an exception. Even though TNT appears to be an especially effective quencher, its spectrum on protected gold shows additional structure that is not seen in the case of the other nitro explosives. It could be speculated that the electronic structure of any ground-state complex formed between TNT and the protected gold surface differs somehow from the complexes formed between the surface and the other nitro explosives studied.

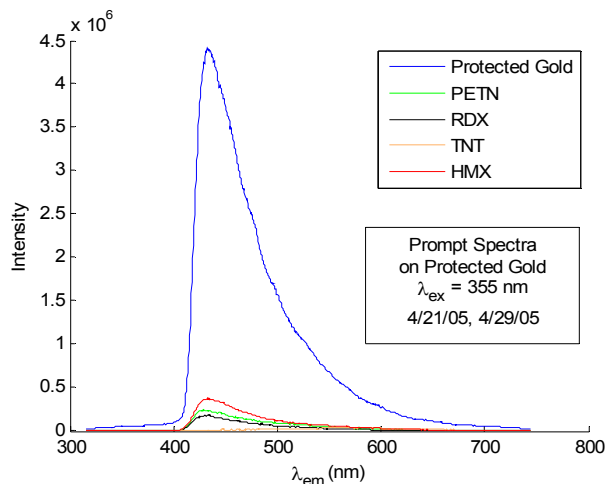


Figure 18. Intensity drop caused by application of nitro explosives to gold surface

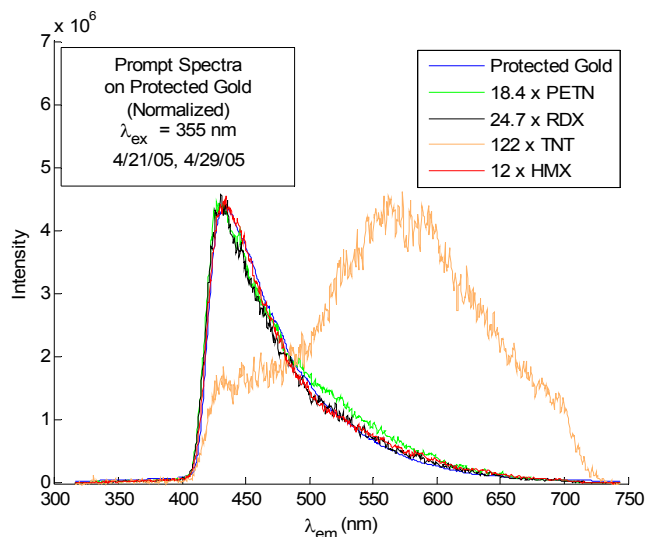


Figure 19. Prompt Spectra on Protected Gold

3.2.2.2 Delayed Spectra

When the time delay after excitation is 100 ns, a quenching effect of the protected gold delayed luminescence similar to that of the prompt luminescence is seen. Figure 20 shows the delayed spectra of protected gold itself and after the application of various nitro explosives at an excitation wavelength of 355 nm.

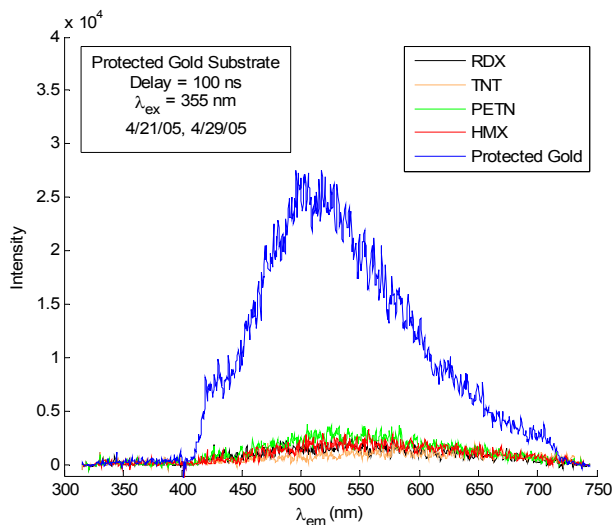


Figure 20. Protected Gold Substrate

3.2.3 Spectra Obtained on Other Substrates

As mentioned previously, fluorescence quenching can be used as an indirect detection method for the presence of nitro explosives. Because of the large extent of fluorescence quenching seen for the protected gold substrate, the team wanted to test the viability of using static quenching in the solid state as an indirect method for remotely detecting nitro explosives on common surfaces. Therefore, explosives fingerprints were applied to a painted metal surface and to a sample cut from a commercial vehicle. These substrates also experienced a quenching effect from the TNT, but the magnitude of the quenching was less pronounced.

3.2.3.1 Painted Metal

A metal surface coated with a latex-based paint was selected as an example of a generic real-world substrate. The effects of TNT on the fluorescence of this substrate are shown in Figure 21. The diminution of the fluorescence intensity is much less dramatic than the quenching effects seen on protected gold.

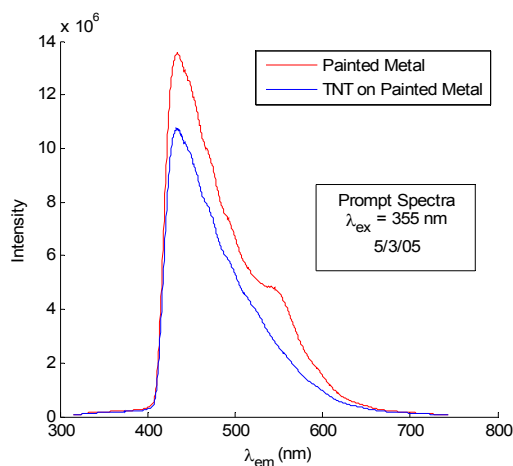


Figure 21. Effects of TNT on the fluorescence of painted metal

3.2.3.2 Vehicle Surface

A sample substrate taken from the door of a U-Haul truck was provided by Tom Neill, shop manager of U-Haul Kargo Repair of Albuquerque. This sample consisted of metal coated with two colors of fluorescent paint and a clearcoat top surface. Figure 22 shows the quenching of the white area of the sample by TNT and RDX at an excitation wavelength of 266 nm, and Figure 23 shows the effect on the orange area. Similar results were seen in the delayed spectra (not shown).

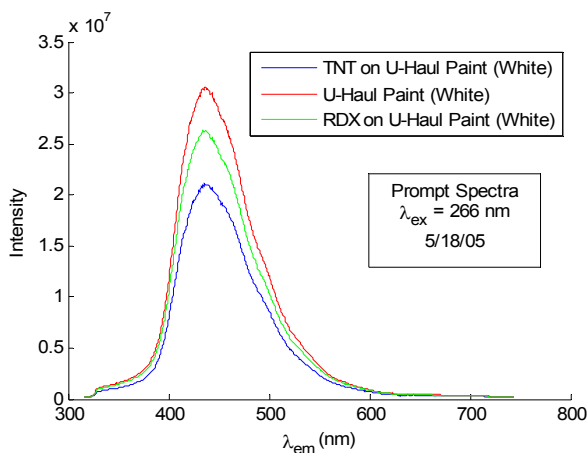


Figure 22. Quenching of the fluorescence of white-painted metal

The surface layer of automotive paint, the clearcoat, is typically 40-50 μm thick (Bertrand-Lambotte et al. 2002) and contains a crosslinked acrylic melamine polymer. It would be expected that, even if the explosives sample quenched the clearcoat fluorescence, the signal from the paint underneath would be unaffected, thereby limiting the degree of signal attenuation obtainable. Even so, appreciable quenching was observed.

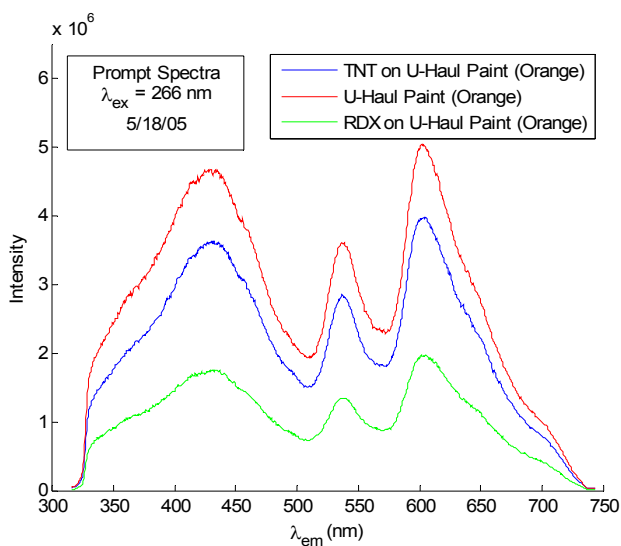


Figure 23. Quenching of the fluorescence of orange-painted metal

3.3 Conclusions Concerning Nitro-Based Explosives

The following conclusions were made from the work with nitro-based explosives:

- Considering only intramolecular electronic processes (those occurring in separated, individual molecules) of the nitro explosives, no photoluminescence is expected from the compounds used under the experimental conditions employed in this study.
- The lack of fluorescence from nitroarenes in the vapor state and in solution is primarily due to fast singlet/triplet intersystem crossing facilitated by the nitro groups.
- Some photodecomposition occurs in TNT, RDX, and HMX when they are excited at a wavelength of 266 nm, which restricts the utility of techniques such as resonance Raman spectroscopy at short wavelengths. However, it might be possible to use 266-nm excitation to study PETN and other nitrate esters without causing deleterious degradation.
- The team cannot definitively state whether the relatively weak photoluminescence signals observed for the nitro explosives on bare gold substrates are due to intrinsic emission from the compounds themselves or to impurities. If there is any intrinsic signal, it must result from intermolecular charge-transfer interactions and/or crystal defect states that are possible only in solids.
- The nitro explosives quench fluorescence on many different surfaces. However, the extent of the static quenching efficiency varies considerably, depending on the nature of the substrate. Therefore, the quenching effect cannot be used as a reliable indirect *in situ* detection method.

4 Ammonium Nitrate/Fuel Oil (ANFO)

4.1 Properties of Individual Components

The following section describes the work on LIF from ammonium nitrate/ fuel oil explosive mixtures. Ammonium nitrate/fuel oil (ANFO) is an explosive mixture of NH_4NO_3 and diesel fuel. The typical weight ratio is 94% ammonium nitrate and 6% fuel oil.

4.1.1 Ammonium Nitrate

Ammonium nitrate (AN) is sold commonly in prill or granular form as a fertilizer. (The surfaces of prills are smooth and glassy, while those of granules are rough.) It is also available as explosives-grade AN, which is more porous and less dense than the fertilizer grade. Pure ammonium nitrate is subject to caking that can cause problems during distribution and use. The material undergoes four solid-state phase transitions between -18 and 125°C ; the temperature-dependent volume changes (especially the 3.6% change occurring at 32°C , or 90°F) (Sjölin 1972) cause cracking, which results in smaller particle sizes. Ammonium nitrate is also hygroscopic, and the small crystallites tend to clump together in a solid mass. In addition, when AN is used as an ingredient in explosives, its caking tendency “adversely affects the sensitivity of the explosive composition and may render it incapable of satisfactory detonation” (Jasnosz 1977). Since it is much more convenient to store and use the AN in the form of small round pellets, anti-caking agents are added to AN to improve its handling properties.

According to a patent issued in 1972, “it has long been common practice” to treat the prills and granules of fertilizer-grade ammonium nitrate with about 0.05 percent of sodium alkyl naphthalene sulfonate (SANS) and about 3 percent powdered clay to form a coating that makes them resistant to caking during storage (Toops, Jr. 1972). Examples of commercially available SANS products are 1) Petro® AG Special powder (a mixture of sodium monomethyl and dimethyl naphthalene sulfonates) (Delmau et al. 2002) from Akzo Nobel Surface Chemistry, and 2) Galoryl® AT additives from ArrMaz Custom Chemicals. Other types of anticaking agents used to coat AN prills are stearic acid or its derivatives and surfactants such as fatty amines, fatty acids, and fatty acid salts carried in an oil-wax matrix (Lawrence and Granholm 2004, Thomas et al. 2002, U.S. International Trade Commission 1998).

Besides functioning as an anticaking coating, SANS can also be added before prilling, where it acts as a “crystal modifier,” making the AN product both porous and strong (Pearson and Morrison 2002). Sodium alkyl naphthalene sulfonates induce pore formation because they are anionic surfactants (Vogel and Monsterleet 2000). In the Kaltenbach-Thuring process for manufacturing explosives-grade AN, the internal additives are water-soluble SANS such as Galoryl® AT 725 or Petro® AG, and the external anticaking additives on the prill surface are oil-soluble anionic fatty amines (Meduselac and Scales 2000, Schapira et al. 1995).

Therefore, the techniques used to produce explosives-grade ammonium nitrate add naphthalene sulfonate salts to the prills—either inside, outside, or both. Since naphthalene sulfonate salts are fluorescent, explosives-grade AN should be fluorescent, especially if broken prills are present. The solution emission maxima of compounds similar to SANS but lacking methyl groups occur at wavelengths from 333 nm to 342 nm when excited at wavelengths between 217 nm and 228

nm (Rose et al. 2001, Rose et al. 2002, Rose et al. 2003). A mixture of mono- and disulfonated naphthalene monomers and their condensed oligomers in aqueous solution shows an emission maximum at about 360 nm when excited at 230 nm (Ruckstuhl et al. 2001, Ruckstuhl et al. 2003). Substituted polyaromatic sulfonates are detectable in water at concentrations in the low parts per trillion by conventional fluorescence spectroscopy techniques (Rose et al. 2001).

Figure 24 shows that both commercially available low-density ammonium nitrate (LDAN) furnished by the Energetics Characterization Department at Sandia National Laboratories and laboratory-grade ammonium nitrate coated with an anti-caking agent exhibit prompt photoluminescence spectra when excited at 266 nm. For comparison, the spectrum of Petro® AG Special powder (sodium alkyl naphthalene sulfonates) is also given. The spectrum of Fluka NH_4NO_3 with purity $\geq 99.5\%$ is extremely weak, showing that ammonium nitrate itself is essentially nonfluorescent.

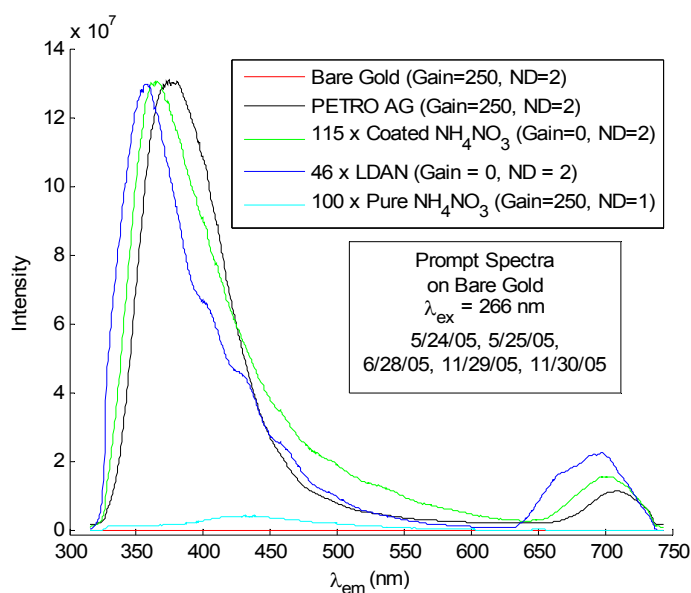


Figure 24. Prompt LIF spectra from pure NH_4NO_3 , coated NH_4NO_3 , low density ammonium nitrate, and Petro AG

The delayed (100 ns) spectra of the substances in Figure 24 are shown in Figure 25. Pure NH_4NO_3 had no discernible delayed spectrum.

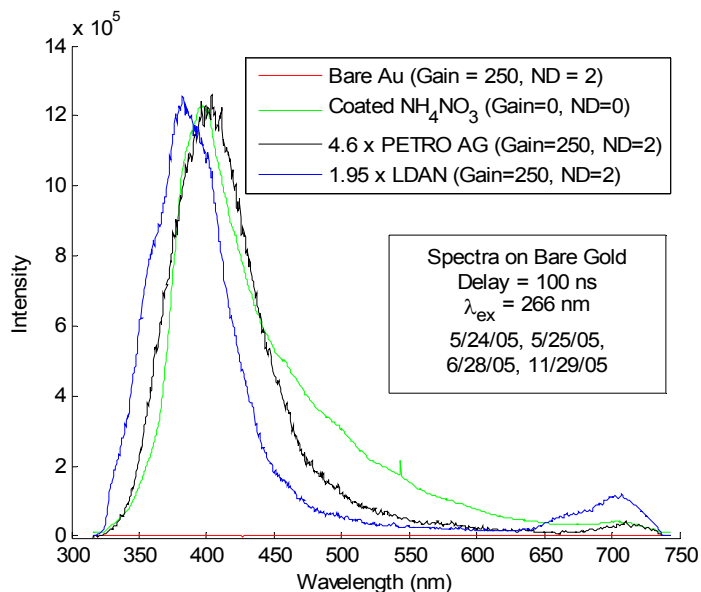


Figure 25. Delayed LIF spectra from pure NH_4NO_3 , coated NH_4NO_3 , low-density ammonium nitrate, and Petro AG

4.1.2 Diesel Fuel

The most common fuel oil used in making ANFO is No. 2 diesel fuel, although kerosene can also be used. Of the over 400 components in diesel fuel, only a few are expected to fluoresce over the wavelength range under observation. The diesel fuel fluorescence is due primarily to the presence of polycyclic aromatic hydrocarbons (PAHs) (Li et al. 2004). Other polycyclic aromatic species, such as sulfur-containing dibenzothiophenes and nitrogen-containing carbazoles, are also fluorescent, but their contribution is relatively small. Most diesel samples excited at wavelengths shorter than 300 nm show a fluorescence emission spectrum that peaks between 350-375 nm with a long-wavelength tail. The main PAHs responsible for the fluorescence are probably alkylated naphthalenes and phenanthrenes, with fluoranthenes and anthracenes contributing to the longer-wavelength region. Figure 26 shows the photoluminescence from diesel fuel obtained from two different sources. The sample labeled “Diesel Fuel” came from the Sandia Labs fueling station, and the one labeled “AccuStandard” is SDF-1X-4 diesel fuel from AccuStandard, Inc. The spectrum of Petro® AG Special powder is also shown to illustrate the similarity of the diesel spectra to that of a naphthalene-based substance. The extra peak at about 411 nm in the AccuStandard fuel sample is apparently caused by a higher concentration of certain PAHs that results in dimer (exciplex) formation, because the intensity of this peak decreases or disappears upon dilution and when the fuel is distributed over powdered materials.

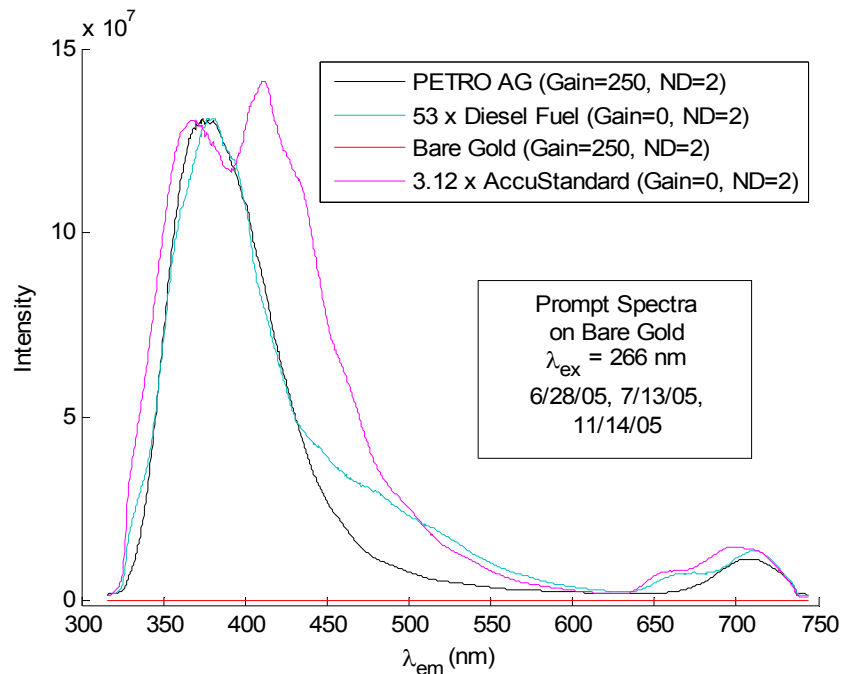


Figure 26. Prompt LIF spectra of diesel fuel, AccuStandard diesel, and Petro AG

The components contributing to the long-wavelength tail in the diesel samples have longer lifetimes than the naphthalene-based portion, as can be seen in the delayed spectra shown in Figure 27 and Figure 28.

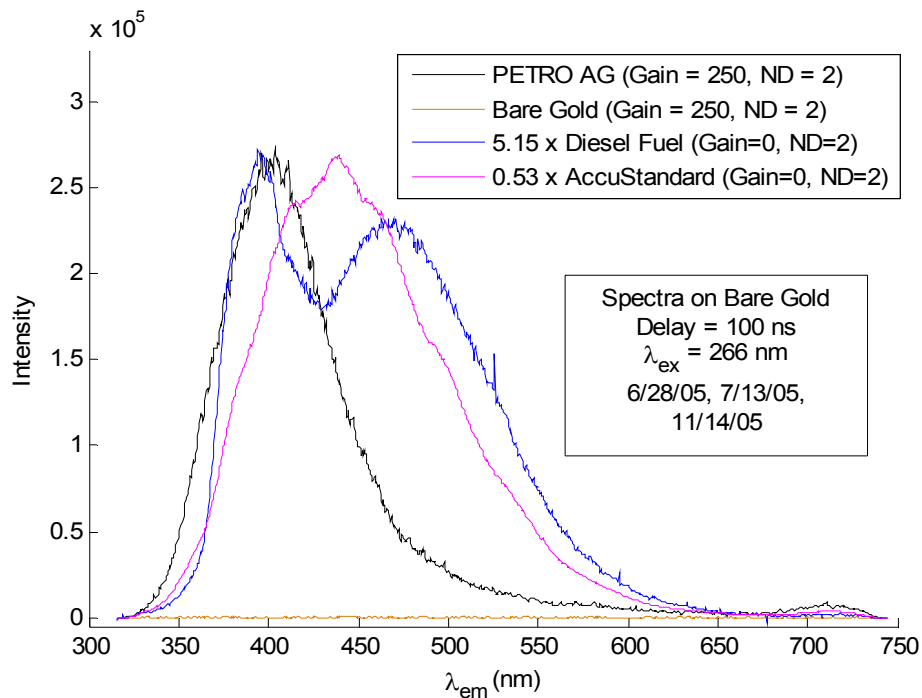


Figure 27. Delayed LIF spectra of diesel fuel, AccuStandard diesel, and Petro AG

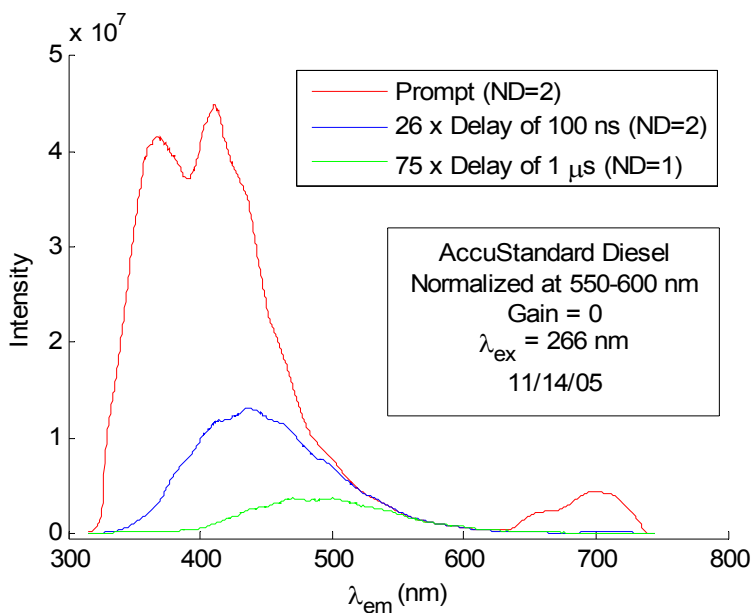


Figure 28. Prompt and delayed LIF spectra of AccuStandard diesel.

Figure 29 shows that there is little effect of excitation wavelength on the AccuStandard diesel emission.

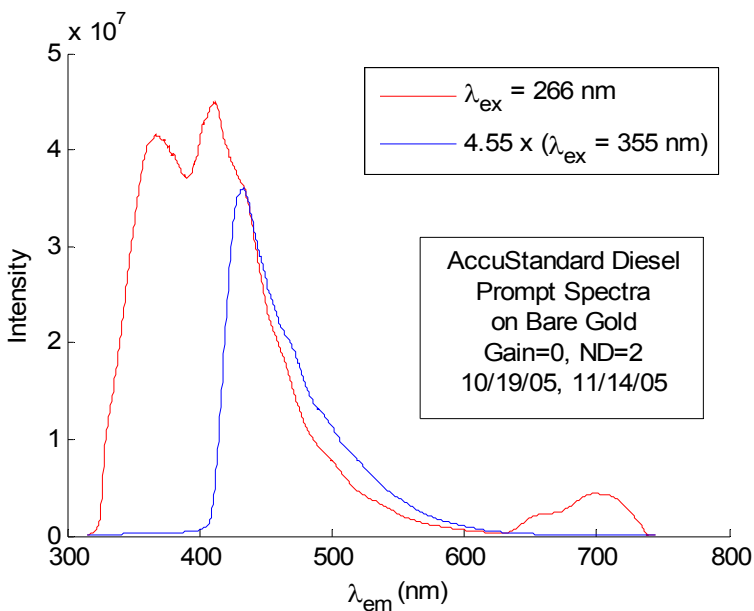


Figure 29. Prompt LIF spectra of AccuStandard diesel comparing 266-nm and 355-nm excitation.

4.2 Photoluminescence of ANFO

The ANFO sample shown in Figure 30 was prepared by 1) crushing the SNL low-density ammonium nitrate in a mortar and pestle, 2) adding Sandia diesel fuel, and 3) stirring the mixture with a glass rod until it was uniform. This sample will be referred to as ANFO1. The weight percent of diesel fuel was 7% instead of the more common 6% formula. The ANFO1 photoluminescence profile is much more similar to the diesel fuel spectrum than to the crushed LDAN spectrum. The differences between the ANFO1 and diesel fuel spectra may indicate that certain components of the diesel are preferentially adsorbed to the surface of the LDAN.

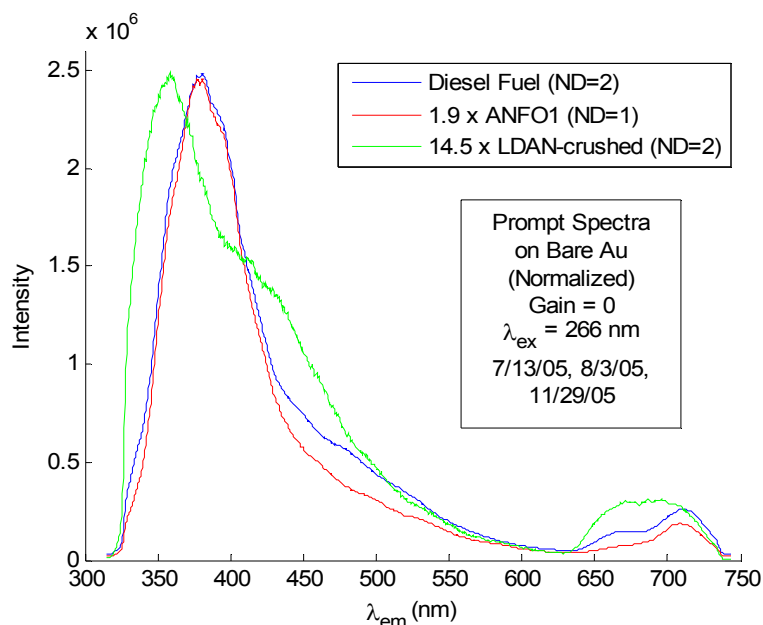


Figure 30. Prompt LIF spectra of diesel fuel, ANFO1 sample, and low density ammonium nitrate (266-nm excitation).

An ANFO2 sample was prepared by adding AccuStandard diesel fuel to the Rodacy LDAN (whole prill). The weight percent of diesel fuel was 6.2%. A comparison of the normalized photoluminescence spectra of ANFO2, AccuStandard diesel fuel and LDAN prill is shown in Figure 31. As with ANFO1, the spectrum of ANFO2 is dominated by the diesel fuel fluorescence.

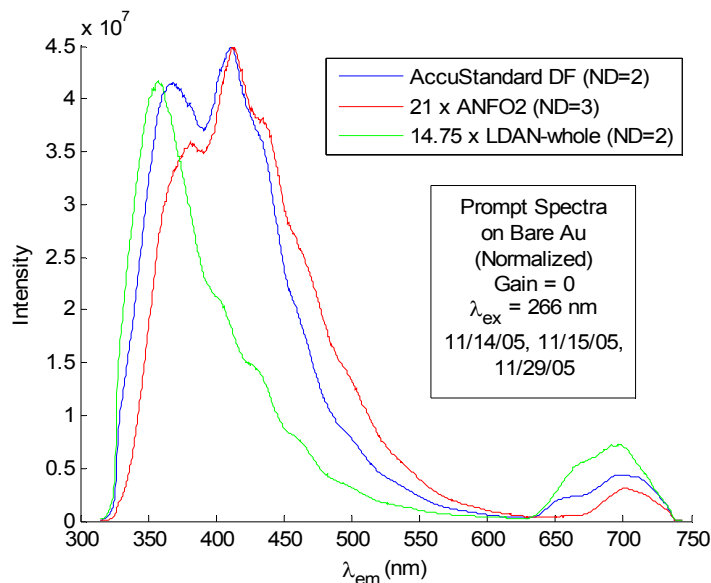


Figure 31. Prompt LIF spectra of AccuStandard diesel, ANFO2 sample, and low density ammonium nitrate (266-nm excitation).

The delayed spectra of ANFO1 and its components are given in Figure 32, and the delayed spectra for ANFO2 (made from the AccuStandard diesel fuel) and its components are shown in Figure 33. As with the prompt spectra, both ANFO delayed spectra are dominated by the diesel fuel contribution.

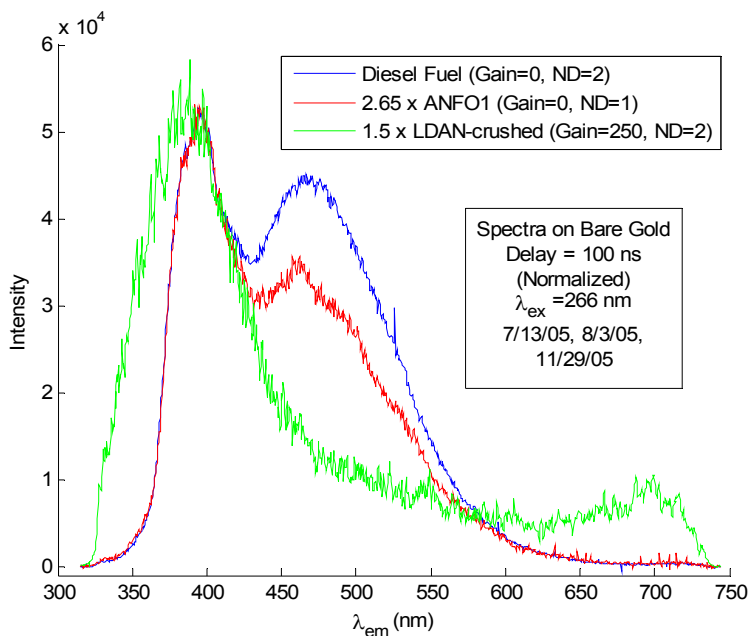


Figure 32. Delayed LIF spectra of diesel fuel, ANFO1 sample, crushed LDAN (266-nm excitation)

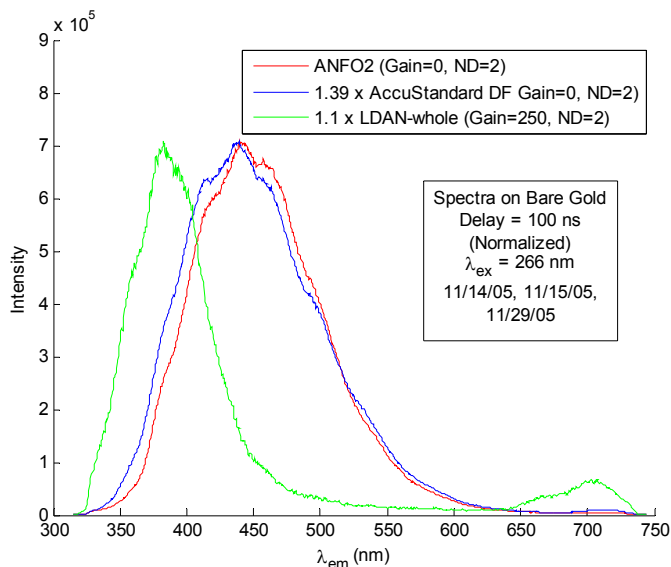


Figure 33. Delayed LIF spectra of ANFO2 sample, Accustandard diesel, and whole LDAN prills (266-nm excitation)

4.2.1 Effect of Particle Size on Prompt Spectra

The appearance of the prompt spectrum of ANFO depends on whether the diesel fuel is distributed over the surface of a whole prill or over finely divided (powdered) prill material. As mentioned in Section 4.2.1, the intensity of the peak at about 411 nm in the AccuStandard diesel fuel spectrum is decreased as the particle size decreases (i.e., as the surface area increases). Figure 34 shows that this peak diminishes when a prill of ANFO2 is crushed. If the LDAN is powdered prior to the addition of the diesel fuel, then the effect is greater; in fact, the extra peak disappears.

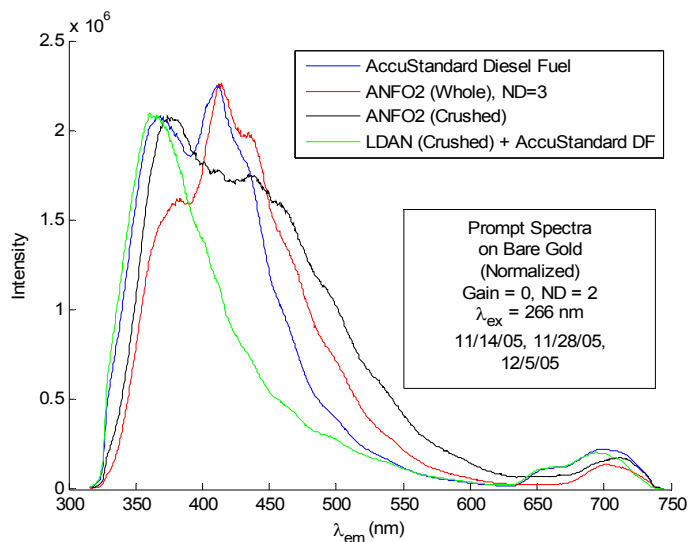


Figure 34. Prompt LIF spectra of AccuStandard diesel, ANFO2 (whole and crushed) and LDAN (266-nm excitation)

Figure 35 shows that the effect caused by the finely divided material is not specific to ammonium nitrate. Similar prompt spectra are seen when powdered sodium chloride or kaolin is used as the support material.

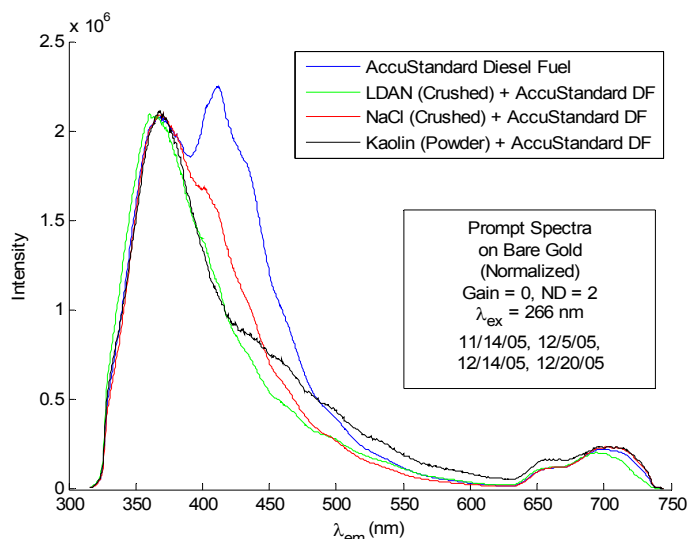


Figure 35. Prompt LIF spectra of Accustandard diesel, LDAN (crushed), NaCl (crushed), and Kaolin (powder) (266-nm excitation).

4.2.2 Delayed Spectra

In general, it appears that the photoluminescence lifetime of the adsorbed diesel fuel is prolonged in comparison with diesel fuel simply applied to a gold surface. An illustration of this effect is shown in Figure 36: the signal intensity persists longer for the ANFO samples than for the diesel fuel alone. At first, the team believed that this observation could possibly be used to distinguish ANFO from either of its components. However, the lifetime effect is variable and difficult to quantify. The magnitude of the effect depends on the particular composition of the diesel fuel used, and differing results are obtained even within the same sample, depending on the location being excited. There are also indications that the smaller the particle size of the support material, the longer the lifetime, but this effect is also highly dependent on the specific parameters of the experiment. The results may also be complicated by the tendency of LDAN to undergo some degree of photobleaching (loss of signal) if the laser power is above a certain threshold value.

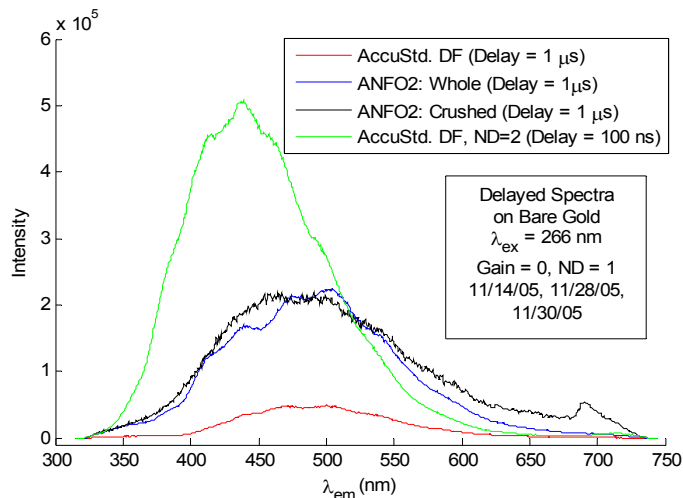


Figure 36. Delayed LIF spectra of AccuStandard diesel and ANFO2 (whole and crushed) (266-nm excitation)

4.3 Conclusions Regarding Ammonium Nitrate/Fuel Oil

The following conclusions were made from the analysis:

- Commercial explosives-grade, low-density ammonium nitrates fluoresce because of substances such as organic surfactants that are added during the manufacturing process.
- Diesel fuel fluorescence is due primarily to the presence of polycyclic aromatic hydrocarbons. Since the relative amounts and identities of the PAHs are specific to a particular fuel sample, the photoluminescence characteristics of diesel spectra will vary.
- The fluorescence spectra of ANFO samples depend mainly on the spectra of the diesel fuel used to prepare them.
- The ANFO spectra can show differences, depending on whether the ammonium nitrate prill is whole or powdered.
- The particle size dependence is not specific to ammonium nitrate. It has been duplicated with another salt (sodium chloride) and with an aluminosilicate (kaolin).
- The photoluminescence lifetimes are quite dependent on the experimental parameters. In general, however, the lifetime of the diesel fuel appears to be prolonged when it is adsorbed onto a support medium such as an ammonium nitrate prill or powder.
- We were unable to discover a method using LIF that would reliably distinguish among ANFO and other materials, such as diesel fuel mixed with road dust.

5 Polarization Effects

Although fluorescence is generally an isotropic process, in some cases the structure of the molecules and/or their interactions with the surfaces they contact can produce an anisotropy with respect to polarization in the absorption or emission process (i.e., either preferentially absorbing one polarization state or preferentially emitting in one polarization). In some cases, fluorescence polarization measurements can provide information about molecular orientation; for example, polarization data have been used to derive details about the sizes and shapes of proteins (Lakowicz 1999). Fluorophores preferentially absorb photons whose electric vectors are aligned parallel to the transition moment of the fluorophore. If, for some reason, the molecules are oriented nonrandomly, the fluorescence emission will be at least partially polarized. Because the NO_2 groups can interact fairly strongly with the surfaces they contact, we conjectured that the presence of nitro-based explosives might result in a fairly well-defined preferred molecular orientation. Such an effect would be expected to be especially noticeable in the case of nitroaromatics such as TNT, which are highly anisotropic. Unfortunately, TNT itself has little (if any) intrinsic fluorescence. However, TNT appears to form complexes with the materials to which it adheres and could conceivably cause detectable differences in the polarization of the fluorescing medium.

Figure 37 shows the polarized photoluminescence spectra for pyrolytic graphite, an extremely anisotropic material. (It also exhibits very little fluorescence, so the intensities are low.) In this section, we label the spectra with two characters (ss, pp, sp, or ps) which indicate the orientation of the excitation polarization (either s or p) and the orientation of the analyzer polarizer (again, either s or p). For example, the “ss” notation refers to the situation in which both the excitation laser beam polarization and the detector (analyzer) polarizer are oriented parallel to the sample. The “sp” notation means that the detector polarizer is turned 90° with respect to the excitation laser beam polarization. (See Section 2.1.) The maximum intensity of the sp arrangement is about half that of the ss. This indicates that the polarized light absorbed by the pyrolytic graphite is still partially polarized when emitted.

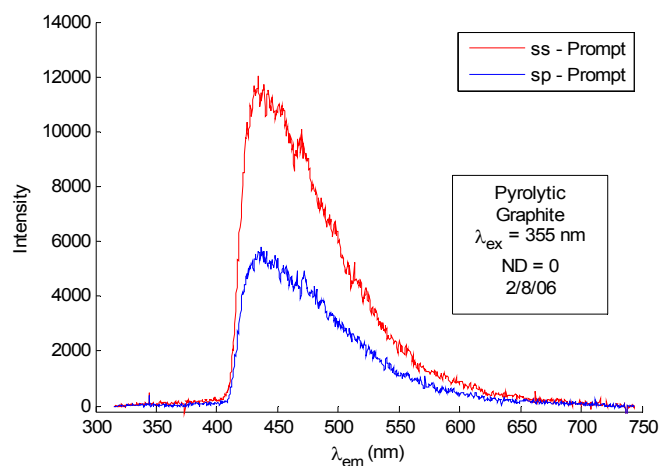


Figure 37. Polarized luminescence spectra for pyrolytic graphite

Similar results were observed in the case of a protected gold surface. Figure 38 shows all four possible configurations (ss, sp, pp, ps) for protected gold. For protected gold, the ss and pp (0°) polarization arrangements yield similar spectra, as do the two cross-polarized (90°) sp and ps setups. Whether the polarization of the input beam is perpendicular or parallel to the plane of incidence does not have much effect on the spectra of protected gold. In general, however, the ss configuration gave higher intensities than pp for several different surfaces that were examined. This means that polarization aligned perpendicular to the plane of incidence (i.e., parallel to the plane of the sample substrate) tended to produce slightly higher signal levels.

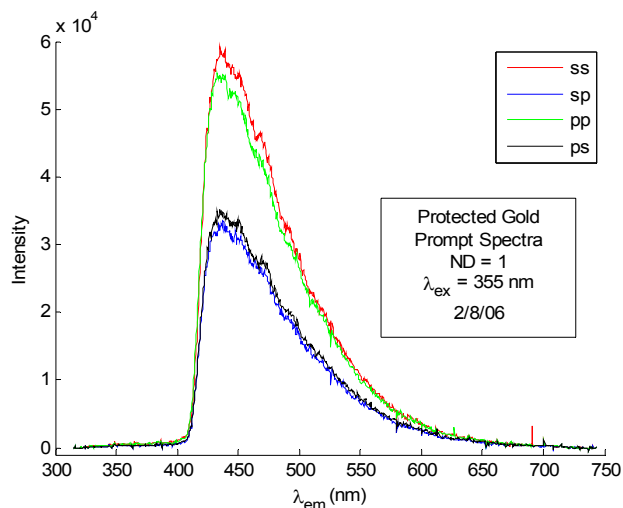


Figure 38. Four possible configurations for protected gold

The degree of surface roughness correlates with loss of signal polarization (Popil 1992). For example, Figure 39 shows the polarized spectra for a material possessing a very rough, isotropic, fluorescent surface—namely, a facial tissue.

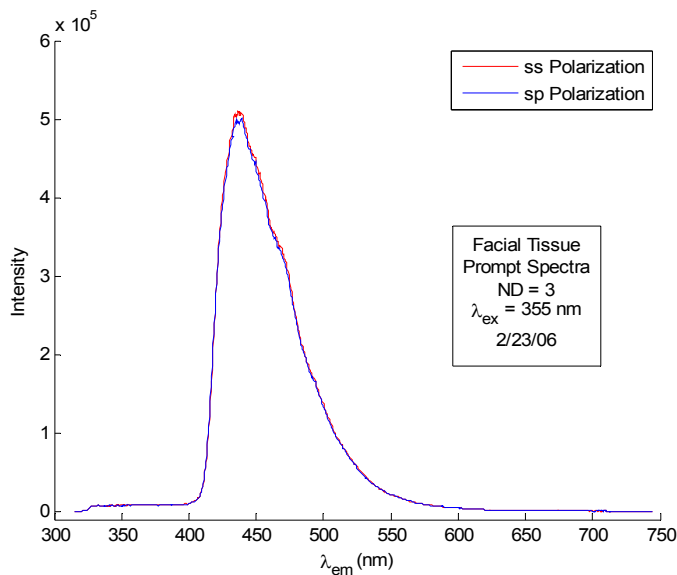


Figure 39. Polarized spectra for a facial tissue

The polarized photoluminescence spectra of a PETN fingerprint on protected gold are shown in Figure 40. The relative order of the ss, sp, pp, and ps intensities are the same as in protected gold itself, but the extent of the signal polarization (difference between the 0° and 90° intensities) has decreased. The decreased polarization could be due simply to the presence of the PETN powder, which would increase the surface roughness.

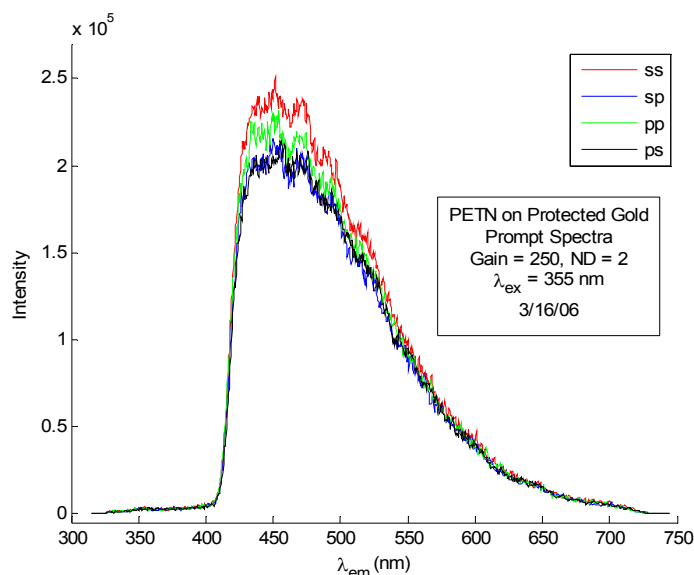


Figure 40. Polarized photoluminescence spectra of a PETN fingerprint on protected gold

The case of TNT on protected gold is shown in Figure 41, Figure 42, and **Error! Reference source not found.**, which are from different locations on the same sample. As with PETN, the degree of polarization anisotropy of fluorescence emission is lessened for the TNT samples compared with that of protected gold.

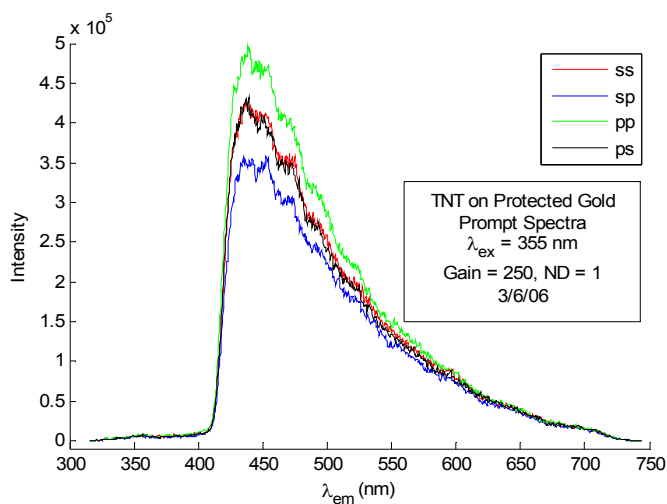


Figure 41. TNT powder in Position 1

In Figure 41 (Position 1), the pp/ps spectra are of higher intensity than the ss/sp spectra, meaning that higher signal resulted when the polarization direction of the input beam was aligned parallel to the plane of incidence. So, in Position 1 it appears that the fluorescence from the s-configuration is quenched slightly more than that from the p-configuration.

Figure 42 shows Position 2, which was a location at which a relatively intense signal was observed. This presumably indicates that the protected gold was less densely covered by TNT in this region. In Position 2, there is an unusual reversal of the pp and ps intensities; the signal is higher in the 90° cross-polarized orientation than in the 0° configuration, which could mean that in Position 2, an input beam with the p-configuration is preferentially quenched. TNT crystals are dichroic, meaning that the absorption of polarized light is a function of the angle between the plane of polarization and the crystalline c-axis (Downs and Forsyth 1973). If a portion of the crystals in the TNT powder at Position 2 happened to adopt a certain orientation with regard to the protected gold surface, perhaps this could explain the results shown in Figure 42.

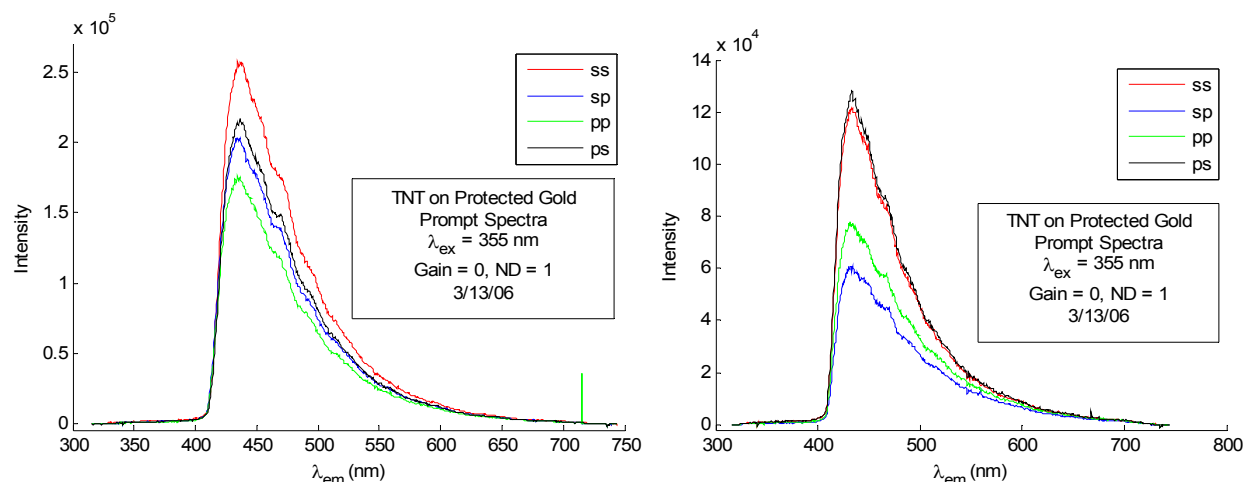


Figure 42. TNT Powder at Position 2, left and Position 3, right

Figure 42 also shows Position 3, which is near Position 2, but with lower intensity, implying that the TNT coverage is probably more dense. Compared with Position 2, the ss/sp separation is wider, and the reversal of the pp and ps intensities is even more pronounced. This situation is caused primarily by the faster attenuation of the sp and pp curves.

5.1 Conclusions from Polarization Studies

- No notable polarization effects were seen in the photoluminescence spectra of PETN on protected gold.
- In the case of TNT on protected gold, polarization effects were present, but they did not appear to be very reproducible or of sufficient magnitude to be usable as a detection method.

6 Spectroscopic and Micrographic Fluorescence Surveys

The team also performed spectroscopic investigations to complement the studies that used laser excitation. These included UV-visible absorption spectra, conventional UV-excited/dispersed fluorescence and UV-excited microscopy. The task was performed

- 1) to provide spectroscopic fluorescence surveys of the explosives studied using broadly tunable UV excitation sources as compared to the laser excitation studies that were limited to a small number of fixed wavelengths (generally harmonics of the 1064-nm fundamental Nd:YAG wavelength, specifically, 355 and 266 nm) and
- 2) to determine the existence of particle-type effects that might enhance fluorescence.

The team obtained a broad overview of the absorption and fluorescence spectra of the explosives studied as a thoroughness check to ensure that there were no significant spectral features that could be used for detection that were not revealed in the laser studies. In contrast to the laser studies, a continuous rather than a pulsed light source was used. As such, these spectra were representative of the steady-state spectroscopic properties rather than of the time-resolved properties. In addition, this study examined the UV-excited fluorescence of explosives microscopically to determine if particle size or crystal habit effects could enhance or otherwise affect the UV-excited fluorescence.

6.1 Explosives Studied and Sample Preparation

This task used samples of RDX, HMX, TNT, PETN, and ANFO. We studied both solid explosives deposited from solution and solutions of the solid samples. The standard solutions¹ consisted of the solid explosive dissolved in a 1:1 mixture of methanol (CH₃OH) and acetonitrile (CH₃CN) for RDX, HMX, TNT, and methanol only for PETN. All of these solutions were very dilute, having a concentration of 0.1 mg explosive per 1 ml solvent.

The solid explosives samples were studied by depositing them onto fused silica, microscope cover slips. Prior to coating with explosive, the cover slips (25 mm x 25 mm x 0.125 mm, Technical Glass Products, Inc.) were cut so that they would fit diagonally into the standard 1-cm cuvette holder of the fluorescence instrument. They were cleaned by radio frequency, argon-ion sputtering for 10 minutes at 0.1-Torr Ar. The cleaning step was needed since all cover slips in the as-received condition showed weak fluorescence.

The solid samples of RDX, HMX, PETN, and TNT were prepared by making saturated solutions using small quantities of explosives (about 10 mg) and small quantities of acetone or acetonitrile (1 to 5 ml) in the barrel of a syringe. After agitating for 1 to 2 minutes, the solution was forced through a 0.1- μ m filter under the pressure of the syringe plunger and deposited onto cleaned, fused silica microscope cover slips. The solid explosives were left behind after the solvent evaporated.

¹ Available from AccuStandard, http://www.accustandard.com/asi/contact_us.php3

The ANFO samples were prepared by adding diesel fuel to explosives grade (i.e., low-density), prilled ammonium nitrate. The spherical prills were typically 1.2 to 1.5 mm in diameter. We used diesel fuel acquired from AccuStandard as described elsewhere in this report. We examined diesel fuel exposed to, then removed from prill, and prill exposed to, and then removed from diesel fuel (#2 fuel oil), as well as prill in contact with excess (greater than 6 wt.%) diesel fuel.

6.2 Absorption Spectra of Explosives

For UV-excited fluorescence to occur, a fluorescent molecule must first absorb a photon, usually at a wavelength that is shorter than the emitted photon that is observed as fluorescence. Thus, light absorption is the first step in the excited-fluorescence process and determines the wavelengths at which a UV-fluorescence explosives detection system would need to operate. Absorption spectra of the various explosives were measured using a Hewlett-Packard Model 8453 absorption spectrophotometer. Typical spectra are shown in Figure 43.

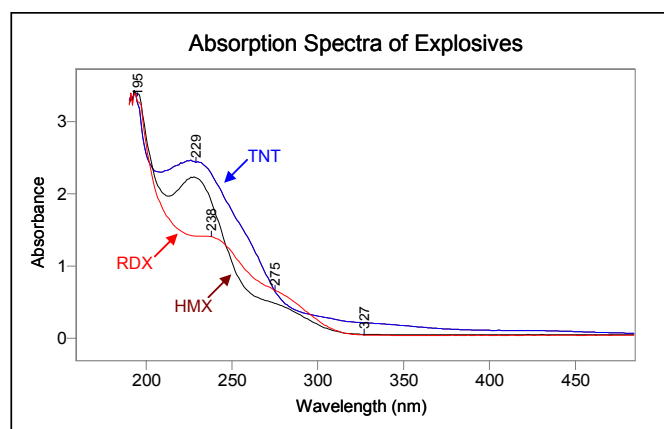


Figure 43. Typical absorption spectra for explosives

All of the explosives show absorption features at wavelengths shorter than 300 nm. However, their absorbance is less than 0.1 at wavelengths longer than 350 nm for all but TNT, which has only a slight absorption that extends out to 450 nm. This suggests that using laser wavelengths around 257 nm or shorter would ensure good coupling of the excitation light to the explosive particles.

6.3 UV-Excited, Dispersed Fluorescence Spectra of Explosives

A Shimatsu, Model 5301PC, fluorimeter was used to measure the dispersed fluorescence of explosives samples. The instrument has two identical monochromators, one for the excitation source and one for the detector. Both monochromators have selectable band widths in six steps from 1.5 to 20 nm; the experiments typically employed a band width of 3 nm for both monochromators. The wavelength of the excitation source can be set at a fixed value or scanned over the spectral region of 200-700 nm. Most of the spectra were taken using a fixed wavelength band and by scanning the detector monochromator to produce dispersed fluorescence spectra. Holding the detection wavelength fixed at the wavelength of a particular emission feature and

scanning the source allows the identification of the excitation wavelengths that produce emission at the fixed detection wavelength. The team recorded spectra of this type for some of the stronger fluorescence bands identified in the project.

In order to minimize the intensity of excitation source light scattered toward the detector, the sample side of the cover slip was oriented away from the detector as illustrated in Figure 44.

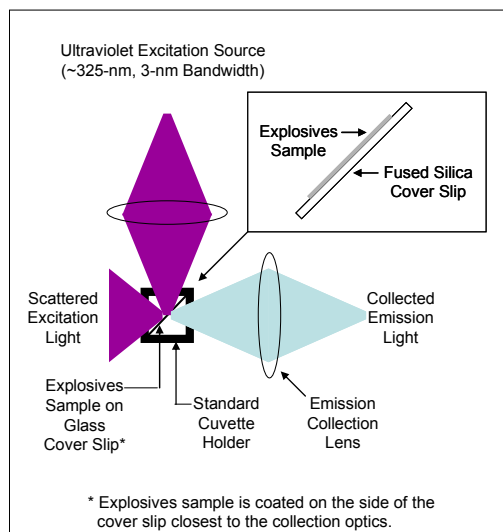


Figure 44. Schematic of how to minimize intensity of light source

The fluorescence spectra of most of the explosives studied was very weak, requiring the highest sensitivity setting available for the fluorimeter. At these high sensitivities, second and third orders of the excitation wavelengths were observed in the dispersed fluorescence spectra. This result was due to overlapping dispersion orders of the detection monochromator. This was more pronounced for the solid samples than for the liquid samples because of increased light scattering due to the solid particles and surface non-uniformities of the solid samples.

6.3.1 Homogeneous Explosives

The excited fluorescence spectra of the various molecular explosives were measured in solutions of methanol/acetonitrile and as dry solids. Even though the primary interest was in spectra of the dry samples, the solution spectra provided better sample uniformity and a check on the dry-sample spectra. In general, a direct comparison between the dry and solution fluorescence spectra cannot be made because analyte-solvent interactions may quench, enhance, or otherwise alter the emission spectra.

The solutions were obtained from AccuStandard at concentrations of 0.1 mg explosive to 1 ml solvent; the solvent was a 1:1 mixture of acetonitrile and methanol. The dry solid samples were prepared from the standard solutions by depositing small amounts onto cleaned, microscope cover slips and allowing the solvent to evaporate. Both glass and fused-silica microscope cover slips were used. However, fused silica (rather than glass) were used for all but the first few spectra because of the interference produced by the natural fluorescence of glass when excited with 325-nm and shorter wavelength light.

Prior to coating with explosive, the cover slips (20 mm x 20 mm x 0.125 mm) were cut to fit diagonally into the standard 1-cm cuvette holder of the fluorescence instrument and cleaned by argon-ion sputtering (10 minutes at 0.1 Torr Ar). The cleaning step was needed since all cover slips in the as-received condition showed weak fluorescence.

6.3.2 Fluorescence Spectra of AccuStandard Explosives Solutions

Figure 45 shows the fluorescence spectra of the AccuStandard explosives solutions described above. The fluorescence spectrum of the RDX sample is very similar to that of the solid RDX shown in the next section.

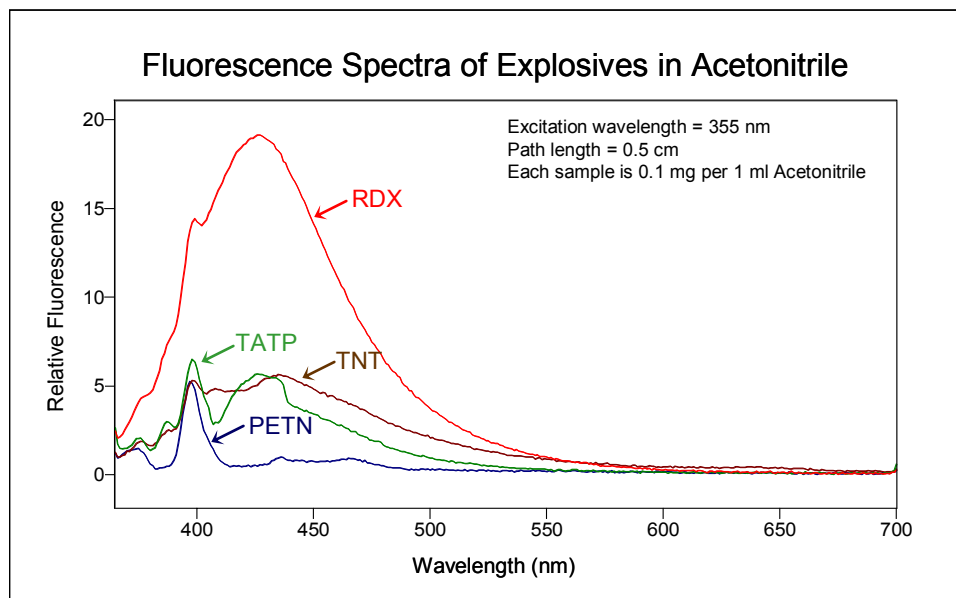


Figure 45. Fluorescence spectra of the AccuStandard explosives solutions

6.3.3 Fluorescence Spectra of Solid (Dry) Homogeneous Explosives Samples

The natural fluorescence of the glass cover slips provided an opportunity to evaluate the fluorescence quenching effect of the nitro-organic explosives reported in the literature and referred to earlier in this report. Adding TNT to the glass cover slips reduced their fluorescence substantially as shown in Figure 46. (Some of the attenuation of the fluorescence signal could be due to the explosive blocking the excitation light from reaching the glass surface; however, the TNT absorption is very weak in this spectral region as can be seen in the figure earlier in this section.) This confirmed the previous reports of the TNT quenching effect. Similar, but less strong quenching effects were observed for the other nitro-organic explosives studied.

Shifting from glass to fused silica cover slips eliminated the background fluorescence problem as illustrated by Figure 47.

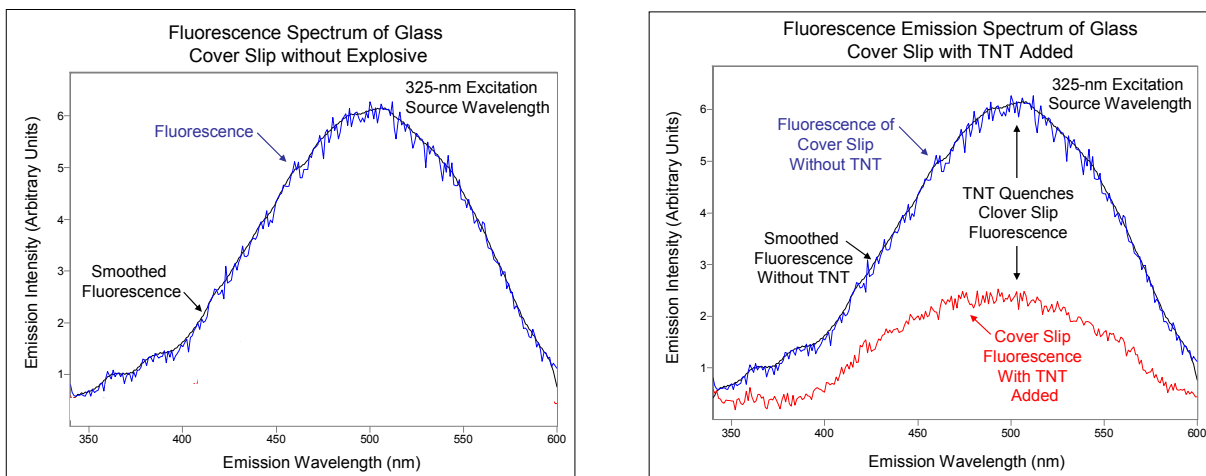


Figure 46. Addition of TNT to the glass cover slips reduced their fluorescence

In general, many more materials fluoresce and their fluorescence is more intense when shorter wavelength excitation is used as compared with excitation with longer wavelength light. Figure 48 shows that there is no significant natural fluorescence from argon-ion sputter cleaned, fused silica microscope cover slips even for the shortest (210 nm) wavelength excitation used in this study.

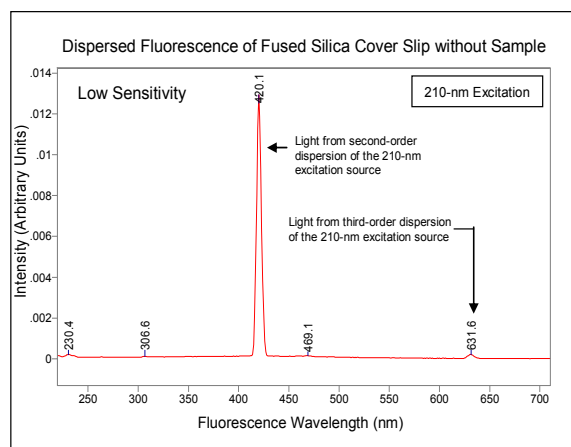


Figure 47. Example of using fused silica cover slips to eliminate background fluorescence

The fluorescence of the solid explosives is extremely weak or undetectable. Virtually no fluorescence was found for samples of solid TNT deposited on fused silica cover slips deposited from acetonitrile solutions. The only significant features in the observed fluorescence spectrum (Figure 48) are due to higher diffraction orders of the excitation source passed by the detection monochromator to the detector.

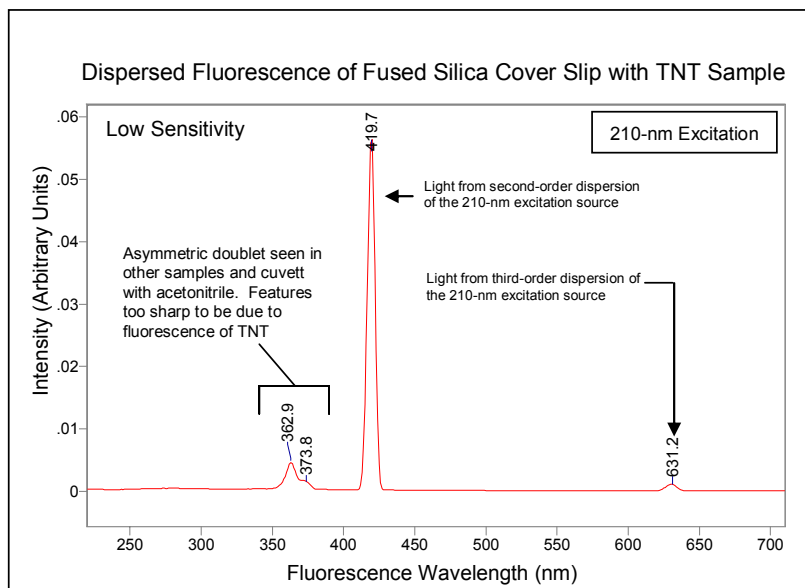


Figure 48. Cleaned cover slips show no natural fluorescence

RDX showed a very weak, broad spectrum when excited with 210-nm light as illustrated by the following two spectra in Figure 49. The figure to the left shows the observed spectrum complete with contamination from higher orders of the excitation light. In the second spectrum (on the right) the spectral features due to the excitation source were removed to obtain a better idea of the RDX fluorescence. The 210-nm excitation spectrum of RDX shows a single, wide fluorescence beginning at about 250 nm, peaking at 403 nm and tailing gradually to about 630 nm. The FWHM is about 173 nm.

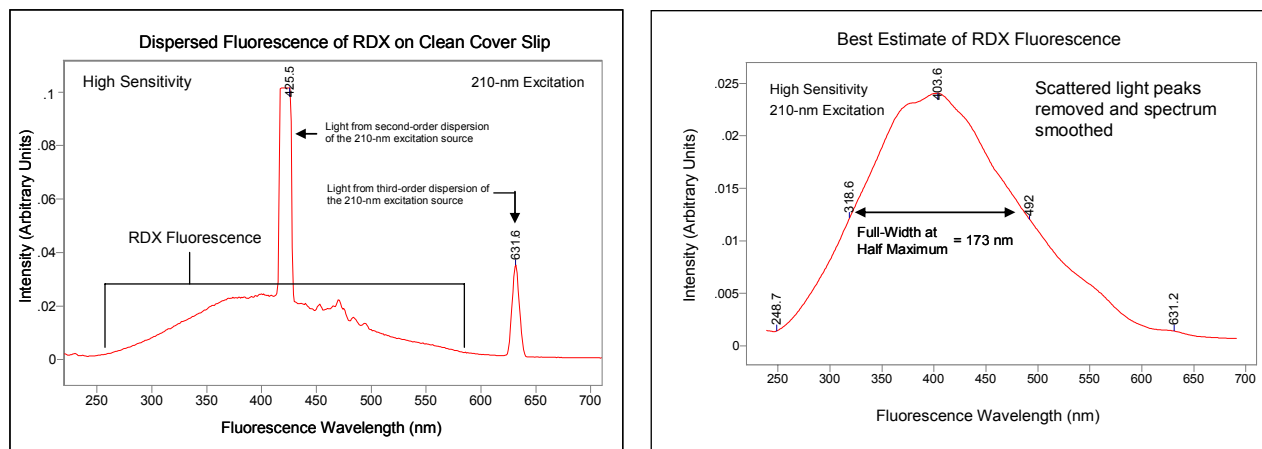


Figure 49. Fluorescence of RDX with 210-nm excitation

The fluorescence spectrum of HMX is very similar to that of RDX but weaker. This result is not surprising since RDX is the trimer and HMX the tetramer of the same nitramine monomer. Somewhat surprisingly, the peak value of the HMX fluorescence is shifted to shorter wavelength (321 nm) relative to RDX (403 nm). Both explosives have fluorescence peaks with long tails skewed toward longer wavelengths. The full-width at half-maximum of the RDX is 173 nm and

that of HMX is 188 nm even though it is more sharply peaked (i.e., the HMX peak is more leptokurtic than the RDX fluorescence). If the central, -C-N-C-N- alternating ring of HMX and RDX were conjugated to form a delocalized π -electron system similar to TNT, the peak fluorescence of HMX would be expected to occur at lower energy, i.e., longer wavelength than that of RDX due to a “particle-in-a-box” effect where the box is larger in the case of HMX and therefore would have lower energy levels. However, the central ring is not conjugated and HMX has a fluorescence maximum that is at a shorter wavelength than RDX and is probably due to more highly localized electron density on the nitrate groups in the case of HMX.

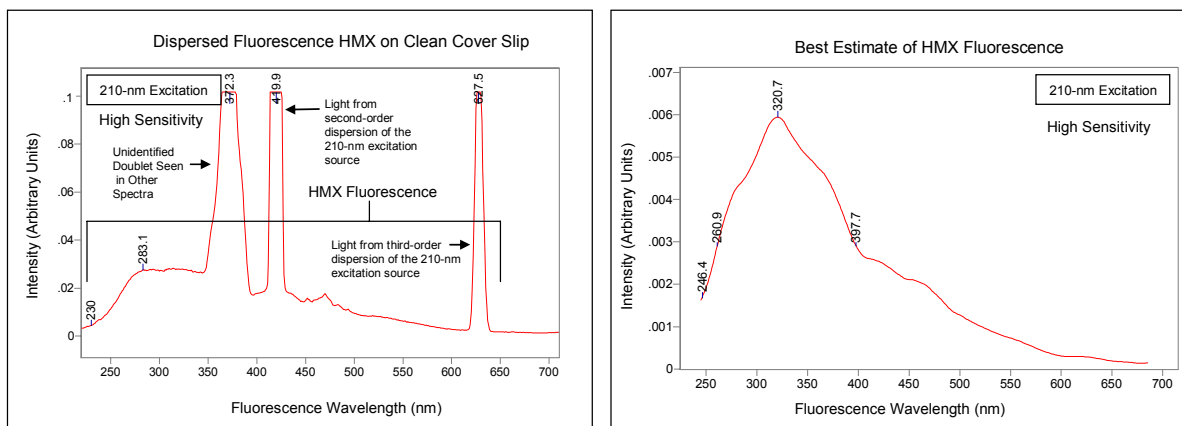


Figure 50. Fluorescence of HMX with 210 nm excitation

PETN shows stronger fluorescence than either RDX or HMX, but nevertheless it is extremely weak. The PETN fluorescence is shown in the next two plots in Figure 51. The fluorescence peak is more symmetrical and slightly more narrow than that of either RDX or HMX.

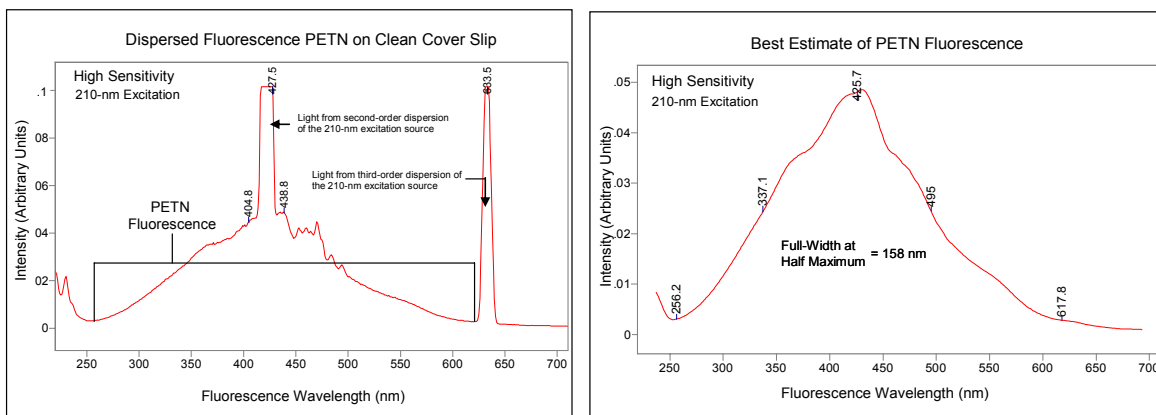


Figure 51. Fluorescence of PETN with 210 nm excitation

6.3.4 Fluorescence Spectra of Heterogeneous Explosives (ANFO)

The fluorescence of ANFO and its components, i.e., the standard diesel fuel mentioned above and explosives-grade prilled ammonium nitrate, were examined. Both the ammonium nitrate prill and the diesel fuel were fluorescent.

A plot of the absorption spectrum and 375-nm excited fluorescence spectrum of the AccuStandard diesel fuel is shown in Figure 52. Although not shown in absolute terms, the fluorescence is moderately bright. The UV absorption is very strong (plotted at 8X so as to be on the same vertical scale with the fluorescence) for wavelengths shorter than 390 nm. In both cases, the path length was 1 cm. Thus, a 1-cm path length of the diesel fuel has an absorbance of 3 at 380 nm, indicating that only 1/1000-th of the incident light at 380 nm passes through a 1-cm path length of the fuel.

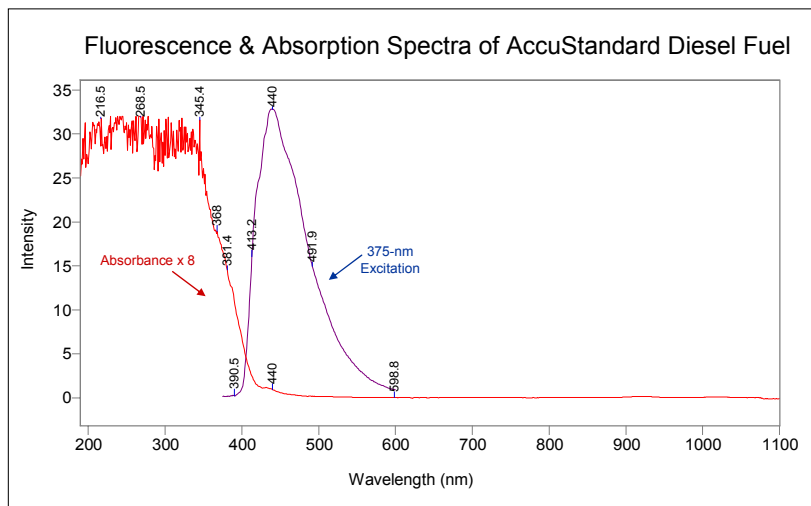


Figure 52. Fluorescence and absorption of AccuStandard Diesel Fuel

Figure 53 shows the fluorescence spectrum of an explosives-grade ammonium nitrate prill soaked with AccuStandard diesel fuel and excited with 210-nm wavelength light. The peak intensity of the fluorescence is near 440 nm and, as in the other fluorescent spectra, the fluorescence exhibits a long tail to long wavelengths.

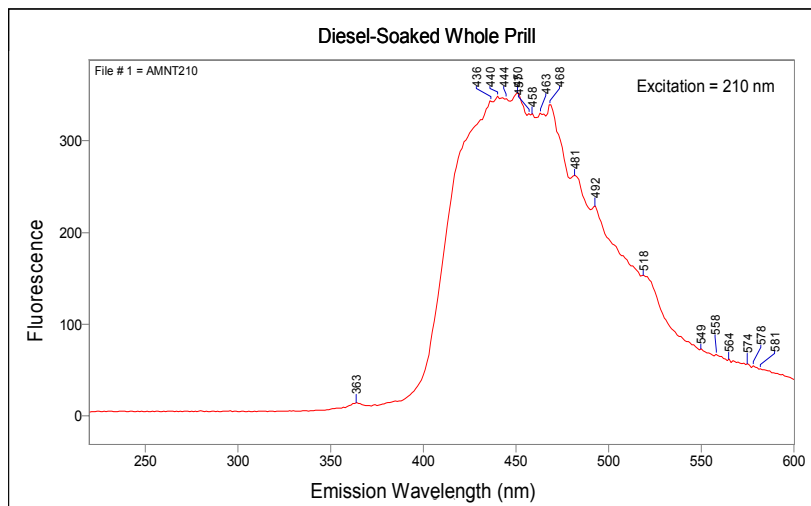


Figure 53. Fluorescence spectrum of an explosives-grade ammonium nitrate prill soaked with AccuStandard diesel fuel and excited with 210-nm wavelength light

The fluorescence spectra of explosives-grade ammonium nitrate was measured without diesel fuel added and with diesel fuel added for various time periods. The results of these studies are summarized in Table 1.

Table 1. Fluorescence of ANFO -ammonium nitrate prill with various exposures to diesel fuel

NOTE: The shaded bands in the table group the same or similar samples; the only difference is excitation at 210 nm or 365 nm.

Sample	Excitation Wave-length (nm)	Fluorescence Peak Value (Arb.)	Peak Center Location (nm)	Half Intensity Point (nm)	Half Intensity Point (nm)	Full-Width at Half-Max. (nm)
Whole prill no diesel exposure	210	605	368	358	380	22
Whole prill no diesel exposure	365	232	431	390	468	78
Whole prill no diesel exposure (repeat)	365	138	431	400	470	70
Whole prill 5-min diesel exposure	210	44	439	405	480	75
Whole prill 5-min diesel exposure	365	610	435	405	475	70
Diesel-soaked whole prill after blotting	210	390	367	357	388	23
Diesel-soaked whole prill after blotting	210	750	366	354	382	28
Diesel-soaked whole prill after blotting	210	580	366	355	380	25
Diesel-soaked whole prill after blotting	365	64	434	405	475	70
Diesel-soaked whole prill (overnight)	210	585	435	404	472	68
Diesel-soaked whole prill (overnight)	365	645	437	409	488	79
Diesel-soaked whole prill	210	340	451	410	515	105
Diesel-soaked whole prill	365	38	438	412	508	96

The fluorescence spectra of the diesel-soaked ammonium nitrate prill show fluorescence maxima around 366 nm with full-width at half-maximum of 25 nm and 434 nm with full-width at half-maximum of 74 nm when excited by 210-nm and 365-nm light respectively. That is, the peak fluorescence shifts to longer wavelength and is more broad when excited with 365-nm light as compared with 210-nm light. This pattern is not followed by the last four samples in the table for which the exposure of the prill to diesel fuel is much longer (hours or overnight). For those samples, the fluorescence peaks at around 440 nm with broader widths of 68 to 105 nm regardless of whether the excitation is at 210 nm or 365 nm. The short wavelength peak seems to have disappeared. This change in the fluorescence spectra with exposure to diesel fuel could form the basis for determining the age of the mixture. However, it is not clear that this would necessarily be useful information for explosives detection.

6.4 Fluorescence Microscopy

ANFO and AN particles were excited with either 365-nm or 475-nm light. A Carl Zeiss, Model 200 M, inverted microscope, with a 20X objective lens and a 10X ocular lens, was used to give a total effective magnification 200X. The excitation source consisted of filtered line emission from a high-intensity mercury vapor lamp. Two different lines were used: one centered at 356-nm having a band pass of 12 nm and a second centered at 470 nm having a bandpass of 20 nm. The images were collected through two additional long-pass filters to give 397-nm long pass images for the first wavelength source and 515-nm long pass for the second source. Photomicrographs were acquired using an Olympus, Model SP-310, 7.1 Megapixel CCD camera.

As shown in Figure 54, the fluorescence from RDX is virtually non-existent when excited by either 365-nm or 470-nm light. Ammonium nitrate produces a faint blue-colored fluorescence when illuminated by 365-nm light but very little when illuminated by 470-nm light.

In a related experiment, we examined reagent-grade ammonium nitrate and observed small regions in the ammonium nitrate crystals that produced a yellow fluorescence that disappeared in less than 2 minutes. There is some evidence that the fluorescence was due to a metallic impurity in the ammonium nitrate that was photo-bleached by continuous exposure to the 365-nm UV excitation source. Native UV fluorescence of ammonium nitrate would be desirable from a detection standpoint, but our studies show that there is none to exploit.

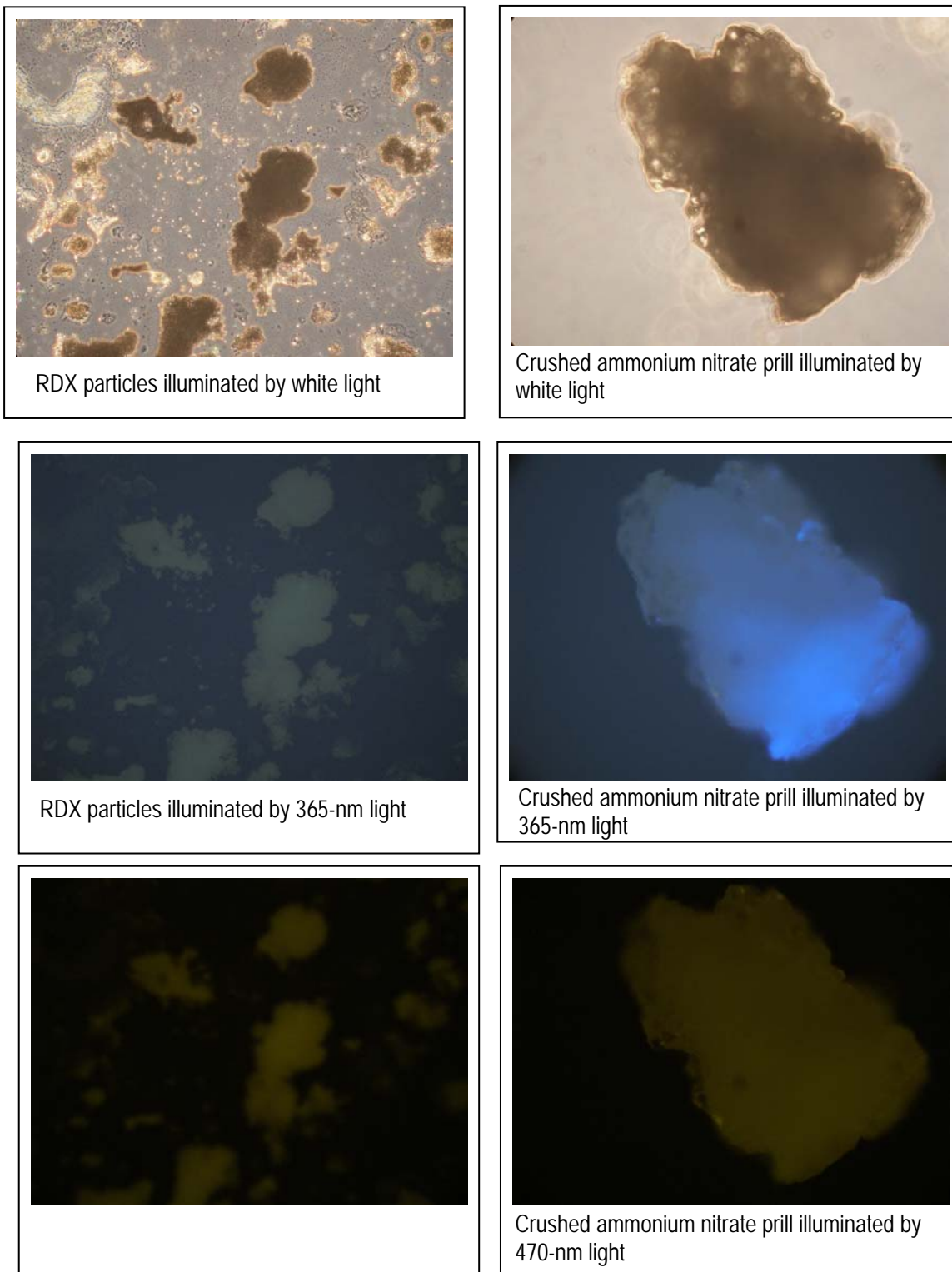


Figure 54. Photomicrographs of RDX and crushed ammonium nitrate prill particles illuminated with white, 365 and 470-nm light

6.5 Conclusions Concerning Fluorescence of Explosives

The following conclusions are made concerning fluorescence of explosives, as measured by standard fluorimetry and fluorescence microscopy:

- The homogeneous explosives (i.e., TNT, RDX, HMX, and PETN) showed moderate to strong absorption at wavelengths shorter than 300 nm.
- Even though the homogeneous explosives had significant absorption, their fluorescence was extremely weak or not detectable. PETN produced the strongest fluorescence, followed by RDX and HMX at about half the intensity of PETN, but even PETN fluorescence is extremely weak.
- The fluorescence from TNT was not detectable even when excited by 210-nm light. However, TNT produced strong fluorescence quenching of materials that are ordinarily fluorescent.
- Explosives that are weakly fluorescent showed a single, asymmetric, broad emission band (full-width at half-maximum of about 180 nm) with the peak fluorescence occurring from 405 to 445 nm and tailing toward longer wavelengths.
- Pure ammonium nitrate is not fluorescent. Some samples of reagent-grade ammonium nitrate showed transitory yellow fluorescence that we believe was due to trace metal impurities in the sample that photo-bleached rapidly.
- Some samples of ammonium nitrate prill can have a coating that we found to be fluorescent. Diesel fuel is fluorescent.
- The mixture of ammonium nitrate and diesel fuel is fluorescent and there are minor changes in the fluorescence of the mixture that occur over a few minutes.
- No aspect of the fluorescence of ANFO could be used to distinguish it unequivocally from diesel fuel alone.

7 Overall Conclusions

In this LDRD we investigated the possibility of using laser-induced fluorescence (LIF) to perform standoff detection of explosives particulates adsorbed on vehicle surfaces. Detection of such particulates could indicate the presence of a vehicle that contains a large mass of explosive material. The explosives studied included 2,4,6-trinitrotoluene (TNT), cyclonite (RDX), octogen (HMX), pentaerythritol tetranitrate (PETN), and ammonium nitrate/fuel oil mixtures (ANFO). The components of ANFO were also studied separately.

Studies of the four nitro-based explosives (TNT, RDX, HMX, and PETN) investigated prompt and delayed fluorescence with excitation primarily at 266 and 355 nm, polarization of both the excitation light and the emitted signals, and fluorescence imaging on a variety of substrates. In

all cases, none of these molecules exhibited any significant native fluorescence. Some weak fluorescence signals were observed that could be due to the compounds themselves or to impurities. This result agrees with the limited number of previous studies in the literature, and with theoretical predictions based on the structures of these molecules. This study revealed that all of these nitro-compounds produce a strong quenching effect when adsorbed on various surfaces, for example, protected gold. However, the magnitude of the quenching effect is highly variable, and it is not limited to nitro-based explosives. It is therefore unlikely that this quenching can ever be exploited to produce a robust and accurate method for the standoff detection of adsorbed explosive particulates. Some polarization effects were also observed, but these also were not consistent enough to provide a reliable “fingerprint” for detection.

Ammonium nitrate fluoresces primarily due to the fuel oil, and in some cases, also due to coating materials and/or impurities that are present in the ammonium nitrate. The spectra show some differences depending on whether the ammonium nitrate is in the form of a whole prill or powdered, a particle-size effect that has been observed with other compounds. In general, there does not appear to be a reliable means of distinguishing between ANFO particles and other materials (such fuel oil mixed with dust particles) based on fluorescence spectra.

These results indicate that it is unlikely that laser-induced fluorescence of adsorbed explosive particulates can be used for the standoff detection of large vehicle bombs. While this study is therefore somewhat disappointing from an applications perspective, it still represents, to the best of our knowledge, the most complete survey of the fluorescence properties of these explosives ever performed and is therefore of considerable interest to the wider scientific community.

Appendix—Table of Absorption/Reflectance Spectral Data

Table A- 1. Summary of Previously Reported Absorption/Reflectance Spectral Data

Nitroarenes		
Explosives	Reference	Solvent in which Spectra Were Taken
Tetryl – Solution	Schroeder et al. 1951	Ethanol
	Abe 1959	Ethanol, water, benzene, acetone
	Thompson 2005	Acetonitrile
Tetryl – Solid	Smith et al. 1984	Reflectance
TNT – Solution	Schroeder et al. 1951	Ethanol
	Abe 1958	Ethanol, water, benzene, acetone
	Abe 1959	Ethanol, water, benzene, acetone
	Conduit 1959	5% Ethanol-water
	Nomura and Abe 1960	Ethanol
	Kamlet et al. 1962	Methanol
	Rothacher et al. 2001	Toluene
	Felt et al. 2002	Water
	Mills et al. 2003	Water
	Gomez et al. 2004	Water, methanol, toluene
	Thompson 2005	Acetonitrile
TNT – Solid	Hummel et al. 2006	Acetonitrile
	Downs and Forsyth 1973	Single crystals
	Smith et al. 1984	Reflectance
TNT – Gas	Osorio Cantillo 2006	Reflectance
	Usachev et al. 2001	
Nitramines		
Explosives	Reference	Solvent in which Spectra Were Taken
HMX – Solution	Schroeder et al. 1951	Ethanol
	Stals et al. 1969	Methanol, ethanol, acetonitrile, water
	Marinkas et al. 1976	Acetonitrile
	Smit 1991	Acetonitrile

Explosives	Reference	Solvent in which Spectra Were Taken
HMX- Solid	Maycock et al. 1969	Single crystal (77 K) and thin film (300 K)
	Marinkas 1975; Marinkas 1977	Single crystal
	Marinkas et al. 1976)	Single crystal reflectance and transmission
	Smit 1991	KCl pellet
RDX – Solution	Schroeder et al. 1951	Ethanol
	Stals et al. 1969	Methanol, ethanol, acetonitrile, water
	Orloff et al. 1970	Acetonitrile
	Stals 1971	Ethanol
	Marinkas et al. 1976	Acetonitrile
	Smit 1991	Acetonitrile
	Qadir et al. 2003	Water
RDX – Solid	Maycock et al. 1969	Thin film,
	Stals 1971	Single crystal and powder (reflectance), Nujol mull (transmission)
	Marinkas 1975; Marinkas 1977	Single crystal
	Marinkas et al. 1976	Single crystal reflectance and transmission
	Smith et al. 1984	Reflectance
	Smit 1991	KCl pellet
Nitrate Ester		
Explosives	Reference	Solvent in which Spectra Were Taken
PETN – Solution	Schroeder et al. 1951	No spectrum observed in ethanol
	Mullen and Orloff 1973	Acetonitrile
	Smit 1991	Acetonitrile
PETN – Solid	Smith et al. 1984	Reflectance
	Smit 1991	KCl pellet
	Dick et al. 1991	Single crystal
	Gruzdkov et al. 2000	Single crystal

NOTE: Borg 1994 contains diffuse reflectance spectra of HMX, PETN, RDX, and TNT, which is of limited utility because most of the reflectance minima are not shown.

References

- Abe, T., 1958. Ultraviolet absorption spectra of nitro-, dinitro-, and trinitro-substituted benzenes. *Bull. Chem. Soc. Jpn.* **31**, 904-907.
- Abe, T., 1959. Substituent effects on the ultraviolet absorption spectrum of 1,3,5-trinitrobenzene in some solvents. *Bull. Chem. Soc. Jpn.* **32**, 339-344.
- Ahmad, S. R. and Foster, V. G., 2000. Pre-resonance Raman scattering in nitrobenzene vapour. *J. Raman Spectrosc.* **31**, 1023-1028.
- Allis, D. G., Prokhorova, D. A., and Korter, T. M., 2006. Solid-state modeling of the terahertz spectrum of the high explosive HMX. *J. Phys. Chem. A* **110**, 1951-1959.
- Berlman, I. B., 1971. *Handbook of Fluorescence Spectra*, edition. Academic Press, New York.
- Bertrand-Lambotte, P., Loubet, J. L., Verpy, C., and Pavan, S., 2002. Understanding of automotive clearcoats scratch resistance. *Thin Solid Films* **420-421**, 281-286.
- Borg, R. A. J., 1994. Diffuse reflectance spectra of energetic material. Report No. DSTO-TR-0065.
- Brand, H. V., 2005. Ab initio all-electron periodic Hartree-Fock study of hydrostatic compression of pentaerythritol tetranitrate. *J. Phys. Chem. B* **109**, 13668-13675.
- Brill, T. B. and James, K. J., 1993. Kinetics and mechanisms of thermal decomposition of nitroaromatic explosives. *Chem. Rev.* **93**, 2667-2692.
- Carper, W. R., Davis, L. P., and Extine, M. W., 1982. Molecular structure of 2,4,6-trinitrotoluene. *J. Phys. Chem.* **86**, 459-462.
- Conduit, C. P., 1959. Ultraviolet and infrared spectra of some aromatic nitrocompounds. *J. Chem. Soc.*, 3273-3277.
- Delmau, L. H., Haverlock, T. J., and Moyer, B. A., 2002. Caustic-side solvent extraction: anti-caking surfactants found to be cause of apparent effect of high nitrite concentration on cesium stripping. Report No. ORNL/TM-2002/104.
- Dick, J. J., Mulford, R. N., Spencer, W. J., Pettit, D. R., Garcia, E., and Shaw, D. C., 1991. Shock response of pentaerythritol tetranitrate single crystals. *J. Appl. Phys.* **70**, 3572-3587.
- Downs, D. S. and Forsyth, A. C., 1973. Optical absorption of TNT single crystals. Report No. PA-TR-4565 (AD-768775).

- Dreger, Z. A., Gruzdkov, Y. A., Gupta, Y. M., and Dick, J. J., 2002. Shock wave induced decomposition chemistry of pentaerythritol tetranitrate single crystals: time-resolved emission spectroscopy. *J. Phys. Chem. B* **106**, 247-256.
- Felt, D. R., Larson, S. L., and Valente, E. J., 2002. UV-VIS spectroscopy of 2,4,6-trinitrotoluene-hydroxide reaction. *Chemosphere* **49**, 287-295.
- Fuh, R. A., 1995. Toluene. Oregon Medical Laser Center, <http://omlc.ogi.edu/spectra/PhotochemCAD/html/toluene.html>. Accessed on 8/25/06.
- Gomez, L. M., Santana, A., Mina, N., Hernandez, S., and Castro, M., 2004. Femtosecond laser UV photochemistry of TNT deposits: the role of hydroxyls. In: Harmon, R. S., Broach, J. T., and Holloway, J. H., Jr. Eds.), *Detection and Remediation Technologies for Mines and Minelike Targets IX*. Proc. SPIE, Bellingham, WA.
- Goodpaster, J. V. and McGuffin, V. L., 2001. Fluorescence quenching as an indirect detection method for nitrated explosives. *Anal. Chem.* **73**, 2004-2011.
- Gruzdkov, Y. A., Gupta, Y. M., and Dick, J. J., 2000. Time-resolved absorption spectroscopy in shocked PETN single crystals. *Shock Compression of Condensed Matter - 1999*,
- Ho, C. K., A. O. Falase, D. W. Hannum, and J. E. Parmeter, *Field and Laboratory Investigations of Factors that Impact the Performance of Trace Explosives Detectors for Vehicle Screening* (UCNI), SAND2004-4748 (2005).
- Hummel, R. E., Fuller, A. M., Schöllhorn, C., and Holloway, P. H., 2006. Detection of explosive materials by differential reflection spectroscopy. *Appl. Phys. Lett.* **88**, 231903-1/231903-3.
- Jasnosz, J. J., 1977. Anti-caking of nitrogenous materials. U.S. Patent 4,001,378.
- Kamlet, M. J., Hoffsommer, J. C., and Adolph, H. G., 1962. Steric enhancement of resonance. I. Absorption spectra of the alkyltrinitrobenzenes. *J. Am. Chem. Soc.* **84**, 3925-3928.
- Karpowicz, R. J. and Brill, T. B., 1983. Librational motion of hexahydro-1,3,5-trinitro-*s*-triazine based on the temperature dependence of the nitrogen-14 nuclear quadrupole resonance spectra: The relationship to condensed-phase thermal decomposition. *J. Phys. Chem.* **87**, 2109-2112.
- Khalil, O. S., Bach, H. G., and McGlynn, S. P., 1970. Luminescence of nitroaromatic molecules. *J. Mol. Spectrosc.* **35**, 455-460.
- Krysanova, O. L., Imamverdieva, L. G., and Aluker, N. L., 2004. Photoluminescence of pentaerythritol and pentaerythritol tetranitrate (PETN). *Proceedings of the 9th International Conference "Physical-Chemical Processes in Inorganic Materials"*, Kemerovo, Russia.
- Kuklja, M. M. and Kunz, A. B., 2000. Ab initio simulation of defects in energetic materials. Part I. Molecular vacancy structure in RDX crystal. *J. Phys. Chem. Solids* **61**, 35-44.

- Kuklja, M. M. and Kunz, A. B., 2001. Electronic structure of molecular crystals containing edge dislocations. *J. Appl. Phys.* **89**, 4962-4970.
- Lakowicz, J. R., 1999. *Principles of Fluorescence Spectroscopy*, 2nd edition. Kluwer Academic/Plenum, New York.
- Lawrence, L. D. and Granholm, R. H., 2004. High density ANFO. U.S. Patent 6,761,781.
- Lee, J., J. E. Parmeter, P. J. Rodacy, D. W. Hannum, M. Mitchell, D. Paul, and C. K. Ho, *Detection of Trace Chemical Plumes from Explosives in Moving Vehicles* (UCNI), SANDOC 2006-6350, Sandia National Laboratories 2006.
- Li, J., Fuller, S., Cattle, J., Way, C. P., and Hibbert, D. B., 2004. Matching fluorescence spectra of oil spills with spectra from suspect sources. *Anal. Chim. Acta* **514**, 51-56.
- Lower, S. K. and El-Sayed, M. A., 1966. The triplet state and molecular electronic processes in organic molecules. *Chem. Rev.* **66**, 199-241.
- Marinkas, P. L., 1975. Luminescence properties of RDX and HMX. Report No. AD-A015538.
- Marinkas, P. L., 1977. Luminescence of solid cyclic polynitramines. *J. Lumin.* **15**, 57-67.
- Marinkas, P. L., Mapes, J. E., Downs, D. S., Kemmey, P. J., and Forsyth, A. C., 1976. Absorption of cyclic polynitramines in the solid and solvated states. *Mol. Cryst. Liq. Cryst.* **35**, 15-25.
- Maycock, J. N., Pai Verneker, V. R., and Lochte, W., 1969. Physico-chemical properties of 1,3,5,7-tetranitro-1,3,5,7-tetrazacyclooctane (HMX). *Phys. Stat. Sol. B* **35**, 849-860.
- Meduselac, M. and Scales, R. C., 2000. Explosive emulsion composition. WO Patent Application 00/17130.
- Mills, A., Seth, A., and Peters, G., 2003. Alkaline hydrolysis of trinitrotoluene, TNT. *Phys. Chem. Chem. Phys.* **5**, 3921-3927.
- Mullen, P. A. and Orloff, M. K., 1973. Ultraviolet absorption spectrum of pentaerythritol tetranitrate. *J. Phys. Chem.* **77**, 910-911.
- Nash, C. P., Nelson, T. E., Stewart, J. J. P., and Carper, W. R., 1989. Molecular structure and vibrational analysis of 2,4,6-trinitrotoluene and 2,4,6-trinitrotoluene- α - d_3 . *Spectrochim. Acta, Part A* **45**, 585-588.
- National Research Council of the National Academies, *Existing and Potential Standoff Explosives Detection Techniques* (2004).
- Nomura, Y. and Abe, T., 1960. Photochemistry of trinitrotoluene. *Kogyo Kagaku Kyokaiishi* **21**, 101-104.

- Ohtani, H., Kobayashi, T., Suzuki, K., and Nagakura, S., 1980. Picosecond spectroscopy studies of the intersystem crossing of aromatic carbonyl and nitro compounds in solution. *Bull. Chem. Soc. Jpn.* **53**, 43-47.
- Orloff, M. K., Mullen, P. A., and Rauch, F. C., 1970. Molecular orbital study of the electronic structure and spectrum of hexahydro-1,3,5-trinitro-*s*-triazine. *J. Phys. Chem.* **74**, 2189-2192.
- Osorio Cantillo, C. M., 2006. Dynamics of TNT photo dissociation studied by femtosecond laser-mass spectroscopy, University of Puerto Rico.
- Pearson, G. R. and Morrison, J. D., 2002. Emulsifiers for explosive compositions. WO Patent Application 02/055184.
- Phelan, J. M., C. K. Ho, L. J. DeChant, P. J. Rodacy, J. Lee, D. W. Hannum, M. Mitchell, and J. E. Parmeter, *Detecting Explosives in Moving Vehicles* (UCNI), SAND2005-6155 (2005).
- Popil, R. E., 1992. Paper roughness or glass sensor using polarized light reflection. U.S. Patent 5,162,660.
- Qadir, L. R., Osburn-Atkinson, E. J., Swider-Lyons, K. E., Cepak, V. M., and Rolison, D. R., 2003. Sonochemically induced decomposition of energetic materials in aqueous media. *Chemosphere* **50**, 1107-1114.
- Rakicioglu, Y., Young, M. M., and Schulman, S. G., 1998. Limitations of quenching as a method of fluorometric analysis of non-fluorescent analytes. *Anal. Chim. Acta* **359**, 269-273.
- Rose, P. E., Benoit, W. R., and Kilbourn, P. M., 2001. The application of the polyaromatic sulfonates as tracers in geothermal reservoirs. *Geothermics* **30**, 617-640.
- Rose, P. E., Johnson, S. D., Kilbourn, P., and Kasteler, C., 2002. Tracer testing at Dixie Valley, Nevada using 1-naphthalene sulfonate and 2,6-naphthalene disulfonate. *Proceedings, Twenty-Seventh Workshop on Geothermal Reservoir Engineering*, Stanford University, Stanford, CA.
- Rose, P. E., Mella, M., and Kasteler, C., 2003. A new tracer for use in liquid-dominated, high-temperature geothermal reservoirs. *Trans. Geotherm. Resources Council* **27**, 403-406.
- Rothacher, T., Lüthy, W., and Weber, H. P., 2001. Interaction of laser radiation with TNT with respect to the laser neutralisation of AP mines. *Appl. Phys. A* **73**, 133-136.
- Ruckstuhl, S., Suter, M. J.-F., and Giger, W., 2001. Rapid determination of sulfonated naphthalenes and their formaldehyde condensates in aqueous environmental samples using synchronous excitation fluorimetry. *Analyst* **126**, 2072-2077.
- Ruckstuhl, S., Suter, M. J.-F., and Giger, W., 2003. Sorption and mass fluxes of sulfonated naphthalene formaldehyde condensates in aquifers. *J. Contam. Hydrol.* **67**, 1-12.

- Schapira, J., Cheminaud, J.-C., Petitbon, P., Guenard, L., and Chaillou, D., 1995. Internal additive and process for the preparation of certain crystallized forms of ammonium nitrate and industrial uses of the said forms. U.S. Patent 5,456,775.
- Schroder, K. L. P. J. Hargis, R. L. Schmitt, D. J. Rader, and I. R. Shokair, "Development of an unattended ground sensor for ultraviolet laser induced fluorescence detection of biological agent aerosols," Proc. SPIE **3855**, 82 (1999).
- Schroeder, W. A., Wilcox, P. E., Trueblood, K. N., and Dekker, A. O., 1951. Ultraviolet and visible absorption spectra in ethyl alcohol. *Anal. Chem.* **23**, 1740-1747.
- Sjölin, C., 1972. Mechanism of caking of ammonium nitrate (NH₄NO₃) prills. *J. Agr. Food Chem.* **20**, 895-900.
- Smit, K. J., 1991. Ultraviolet and visible absorption spectroscopy of some energetic molecules in the solid state. *J. Energ. Mater.* **9**, 81-103.
- Smith, E. M., Aronson, J. R., Cornish, R. M., Goodwin, B. E., Simon, I., and Von Thuna, P., 1984. Surface sampling techniques using ultraviolet illumination. Report No. AMXTH-TECR-84308.
- Stals, J., 1971. Chemistry of aliphatic unconjugated nitramines. Part 4.--Photophysical processes of secondary nitramines. *Trans. Faraday Soc.* **67**, 1739-1748.
- Stals, J., Barraclough, C. G., and Buchanan, A. S., 1969. Molecular orbital interpretation of the ultra-violet absorption spectra of unconjugated aliphatic nitramines. *Trans. Faraday Soc.* **65**, 904-914.
- Takezaki, M., Hirota, N., and Terazima, M., 1997a. Nonradiative relaxation processes and electronically excited states of nitrobenzene studied by picosecond time-resolved transient grating method. *J. Phys. Chem. A* **101**, 3443-3448.
- Takezaki, M., Hirota, N., and Terazima, M., 1998. Relaxation of nitrobenzene from the excited singlet state. *J. Chem. Phys.* **108**, 4685-4686.
- Takezaki, M., Hirota, N., Terazima, M., Sato, H., Nakajima, T., and Kato, S., 1997b. Geometries and energies of nitrobenzene studied by CAS-SCF calculations. *J. Phys. Chem. A* **101**, 5190-5195.
- Thomas, D. R., Ciaccio, C. G., and Collins, K., 2002. Coating agent and coated particulate fertilizers. U.S. Patent 6,475,259.
- Thompson, R. Q., 2005. Forensic Science Laboratory: Identification of organic explosives on plastic surfaces.
<http://www.asdlib.org/onlineArticles/elabware/thompson/Explosives/ExplosSpectra.pdf>.
Accessed on 8/29/06.

Toal, S. J. and Trogler, W. C., 2006. Polymer sensors for nitroaromatic explosives detection. *J. Mater. Chem.* **16**, 2871-2883.

Toops Jr., E. E., 1972. Noncaking, grained ammonium nitrate. U.S. Patent 3,640,697.

U.S. International Trade Commission, 1998. Ammonium nitrate: A comparative analysis of factors affecting global trade. Report No. 3135.

Usachev, A. D., Miller, T. S., Singh, J. P., Yueh, F.-Y., Jang, P.-R., and Monts, D. L., 2001. Optical properties of gaseous 2,4,6-trinitrotoluene in the ultraviolet region. *Appl. Spectrosc.* **55**, 125-129.

Vogel, E. and Monsterleet, J., 2000. Process for producing porous ammonium nitrate and ammonium nitrates produced. U.S. Patent 6,022,386.

Wallenborg, S. R. and Bailey, C. G., 2000. Separation and detection of explosives on a microchip using micellar electrokinetic chromatography and indirect laser-induced fluorescence. *Anal. Chem.* **72**, 1872-1878.

Zeman, S. and Krupka, M., 2003. New aspects of impact reactivity of polynitro compounds, Part III. Impact sensitivity as a function of the intermolecular interactions. *Propellants, Explos., Pyrotech.* **28**, 301-307.

Distribution

2		LDRD Office
1	MS 0782	William G. Rhodes, 06418
1	0782	John E. Parmeter, 06418
1	1423	Carol Phifer, 01128
1	1423	Randy Schmitt, 01128
1	1423	Gregory Hebner, 01128
1	9055	Lawrence R. Thorne, 08134
2	0762	S. Jordan, 06407
2	MS 9018	Central Technical Files, 08944
2	0899	Technical Library, 04536

This page intentionally left blank.